Nonlinear Dynamics **21:** 101–133, 2000.

The Nonlinear Dynamics of Filaments

ALAIN GORIELY and MICHAEL TABOR
Department of Mathematics and Program in Applied Mathematics, University of Arizona, Building #89, Tucson, AZ 85721, U.S.A.

(Received: 8 September 1998; accepted: 22 June 1999)

Abstract. The Kirchhoff equations provide a well-established framework to study the statics and dynamics of thin elastic filaments. The study of static solutions to these equations has a long history and provides the basis for many investigations, both past and present, of the configurations taken by filaments subject to various external forces and boundary conditions. Here we review recently developed techniques involving linear and nonlinear analyses that enable one to study, in some detail, the actual dynamics of filament instabilities and the localized structures that can ensue. By introducing a novel arc-length preserving perturbation scheme a linear stability analysis can be performed which, in turn, leads to dispersion relations that provide the selection mechanism for the shape of an unstable filament. These dispersion relations provide the starting point for nonlinear analysis and the derivation of new amplitude equations which describe the filament dynamics above the instability threshold. Here we will mainly be concerned with the analysis of rods of circular cross-sections and survey the behavior of rings, rods, helices and show how these results lead to a complete dynamical description of filament buckling.

Keywords: Elastic filaments, buckling, looping, dynamical instabilities.

1. Introduction

The classic buckling instability of a thin elastic filament when it is subjected to the appropriate amount of twist, lies at the heart of many important processes ranging from the kinking of telephone cables when they are being laid [1, 2], to the super-coiling properties of long molecular structures such as proteins, DNA and bacterial fibers [3–11]. In addition, long, thin, twisted elastic structures play important paradigmatic roles in the theory of polymers and liquid crystals [12, 13]; characterizing the motion of vortex tubes in hydrodynamics [14]; and modeling the formation of sun spots and heating of the solar corona [15, 16]. These applications have spawned many theoretical and computational studies and have also prompted the development of experimental investigations to help bench-mark the theoretical work. These experimental studies range from the controlled buckling studies of macroscopic elastic rods [17] to the ingenious manipulations of DNA strands [18].

A filament is defined, roughly speaking, to be a three dimensional body whose cross-section is much smaller than its length. If, furthermore, the curvature of the filament is assumed to be small relative to its length, it is possible to show that its dynamics is governed by the celebrated Kirchhoff equations. (An excellent historical study of these equations is provided by Dill [19]). These equations describe the evolution of a filament in (three-dimensional) space and consist of a system of six coupled, nonlinear PDEs of second-order in time and arc-length; the latter variable providing the intrinsic coordinatization of the filament.

A considerable amount of work has been devoted to investigating the stability of given stationary filament configurations [20–22] through the study of the static Kirchhoff equations – which form a much more tractable system of six coupled nonlinear ODEs. As is well known,

these are exact analogues of the Euler equations for rigid-body motion and, accordingly, are often cast in terms of the Euler angles to characterize the orientation of the local basis describing the twisting and bending of the rod (as a function of arc-length). This type of analysis has yielded a very a rich variety of exact solutions from which conclusions about the stability are often drawn.

Analytical study of the full dynamical equations is a very challenging problem and to date has mainly been restricted to the study of traveling wave solutions [23]. An alternative approach has been to introduce a time-dependent Lagrangian to describe elementary vibrations of the equilibrium solutions [24, 25]. However, these Lagrangians are *ad-hoc* models which are not related to the dynamical Kirchhoff equations and do not truly describe the dynamics of real elastic filaments. An alternative to analytical work is provided by numerical simulation – a non-trivial task in its own right – and this approach has been pursued with some success by a number of groups [26–28].

In order to obtain a complete, dynamical, picture of filamentary instabilities we depart from traditional approaches and consider the linear stability of static solutions to the full, three-dimensional, dynamical Kirchhoff model: this is achieved through the development a new arc-length preserving perturbation scheme. The dispersion relations that ensue from the associated linear problem, then provide the starting point for a global *weakly nonlinear analysis* which provides a description of the evolution of unstable structures beyond threshold.

The structure of this review paper is as follows. In Section 2, we briefly review the derivation of the Kirchhoff equations in order to introduce the basic notation. In Section 3, we introduce the perturbation scheme which is developed in terms of the so-called director basis. The fundamental property of this perturbation expansion is that it preserves arc-length (and hence total filament length) at each order of the perturbation. Applying this scheme to the Kirchhoff equations yields variational equations governing the stability of stationary solutions. This approach is illustrated in Section 4 with the examples of the twisted planar ring, the twisted straight rod, and a helical rod. In Section 5 we describe our nonlinear analysis of the Kirchhoff equations and illustrate the technique for the circular ring and the straight rod. The nonlinear analysis of the ring is performed at the level of a single mode, which leads to a nonlinear amplitude equation in the form of a single ordinary differential equation. In the case of the twisted straight rod, which involves a continuum of modes, the analysis leads to amplitude equations which take the form of a pair of coupled nonlinear Klein–Gordon equations. The nonlinear analysis provides vital information about the amplitude of the structures that appear after bifurcation, and is essential for the description of the localization that occurs after buckling. In the remaining three sections of this review we describe a variety of applications of our approach to filament problems. In Section 6 we give a summary of our dynamical model of buckling of a straight rod subjected to twisting forces; and in Section 7 we describe the fundamental role played by intrinsic curvature and twist in the morphogenesis of naturally occurring filaments. Although the earlier parts of this review follow, fairly closely, the presentations given in our recent series of papers [29–33], a variety of new, or previously unpublished, results are sprinkled throughout, especially in the later sections.

2. The Kirchhoff Model

A fundamental idea in Kirchhoff's theory of thin filaments is to represent all the physically relevant stresses, i.e., the forces and the moments, as cross-sectional averages at each point

along the space curve representing the axis of the filament. It is this that enables one to write down a spatially one-dimensional model for a filament.

Let $x = x(s,t) : \mathbb{R} \times \mathbb{R} \to \mathbb{R}^3$ be the space curve, parameterized by the arc-length s, representing the filament axis, whose position can also depend on the time t. The curve is assumed to be at least three times differentiable with respect to s. For each value of s and t, a local, orthonormal coordinate system, called the *director basis*, $\{d_1, d_2, d_3\}$ is associated with the curve by identifying the vector $d_3(s,t) = x'(s,t)$ as the tangent vector of x at s (the prime denotes the s-derivative), and taking the vectors d_1, d_2 to span the plane normal to d_3, such that $\{d_1, d_2, d_3\}$ forms a right-handed triad ($d_1 \times d_2 = d_3$, $d_2 \times d_3 = d_1$). In the case where d_1 is along d_3', the director basis specializes to the well-known Frenet triad where d_1 is the normal vector and d_2 the bi-normal vector. The director basis is more general (and more useful) than the Frenet basis since the vectors $\{d_1(s,t), d_2(s,t)\}$ can be chosen to coincide with the principle axes of the rod cross-section and hence capture the actual twist of the rod itself (rather than just the torsion of the axial space curve).

Given the director basis $\{d_1, d_2, d_3\}$, the filament geometry can be reconstructed at all times by integrating the tangent vector, i.e.,

$$x(s,t) = \int^s d_3(s,t)\, \mathrm{d}s.$$

The *kinematics* of thin filament evolution can be easily written in term of the director basis. Taking into account the orthonormality of this basis, one readily obtains its evolution with respect to arc-length and time; namely

$$d_i' = \sum_{j=1}^{3} K_{ij} d_j, \quad i = 1,2,3, \tag{1a}$$

$$\dot{d}_i = \sum_{j=1}^{3} W_{ij} d_j, \quad i = 1,2,3, \tag{1b}$$

where $\dot{(\,)}$ stands for the time derivative. W and K are the antisymmetric 3 by 3 matrices:

$$K = \begin{pmatrix} 0 & \kappa_3 & -\kappa_2 \\ -\kappa_3 & 0 & \kappa_1 \\ \kappa_2 & -\kappa_1 & 0 \end{pmatrix}, \quad W = \begin{pmatrix} 0 & \omega_3 & -\omega_2 \\ -\omega_3 & 0 & \omega_1 \\ \omega_2 & -\omega_1 & 0 \end{pmatrix}. \tag{2}$$

The elements of K make up the components of the *twist vector*, namely

$$\kappa = \sum_{i=1}^{3} \kappa_i d_i;$$

and the elements of W define the components of the *spin vector*, namely

$$\omega = \sum_{i=1}^{3} \omega_i d_i.$$

The two linear system (1) must be compatible: thus by cross-differentiation one determines that:

$$W' - \dot{K} = [W, K], \tag{3}$$

where [., .] is the matrix commutator: $[W, K] = W.K - K.W$

To go from the kinematics of the director basis to the actual *dynamics* of an elastic rod, we now consider the forces and moments acting in such a rod (here with a circular cross-section) with the axial space curve $x = x(s, t)$. The main physical assumptions considered here are: no shear deformation, no axial extensibility, linear constitutive relationships and circular cross-sections (the case of non-circular cross-sections is considered in detail in [34]). As indicated above, the stresses are averaged over the cross-sections along (and normal to) the central axis: this enables the total force $F = F(s, t)$ and moment $M = M(s, t)$ to be expressed locally in term of the director basis, i.e.,

$$F = \sum_{i=1}^{3} f_i d_i, \quad M = \sum_{i=1}^{3} M_i d_i.$$

Conservation of linear and angular momentum then provides the fundamental equations of motion [35]:

$$F'' = \rho A \ddot{d}_3 \tag{4a}$$

$$M' + d_3 \times F = \rho I (d_1 \times \ddot{d}_1 + d_2 \times \ddot{d}_2) \tag{4b}$$

where I is the moment of inertia (about a radial cross-section), ρ is the density and A the area of a (circular) cross-section.

The equations are completed by the constitutive relationship of *linear* elasticity theory; namely a relationship between the moment and the strains of the form:

$$M = EI[(\kappa_1 - \kappa_1^u)d_1 + (\kappa_2 - \kappa_2^u)d_2] + 2\mu I(\kappa_3 - \kappa_3^u)d_3, \tag{5}$$

where E is the Young modulus and μ the shear modulus and the κ_i^u are the 'intrinsic curvatures' of the filament. For the meantime we will set these to zero (which implies that the rod is 'naturally' straight and untwisted); but we will later discuss how they can provide the fundamental 'driving force' for certain types of spontaneous morphogenesis, e.g., supercoiling of bacterial filaments [36] and the helix-hand reversal seen in the tendrils of climbing plants [37].

The standard scalings

$$\begin{aligned} t &\to t\sqrt{I\rho/AE}, \quad s \to s\sqrt{I/A}, \\ F &\to AEF, \quad M \to ME\sqrt{AI}, \\ \kappa &\to \kappa\sqrt{A/I}, \quad \omega \to \omega\sqrt{AE/I\rho}. \end{aligned} \tag{6}$$

reduce Equations (4) and (5), to the dimensionless form

$$F'' = \ddot{d}_3, \tag{7a}$$

$$M' + d_3 \times F = d_1 \times \ddot{d}_1 + d_2 \times \ddot{d}_2, \tag{7b}$$

$$M = \kappa_1 d_1 + \kappa_2 d_2 + \Gamma\kappa_3 d_3, \tag{7c}$$

where $\Gamma = 2\mu/E = 1/(1 + \sigma)$ characterizes the elastic property of the filament: varying between 2/3 (incompressible case) and 1 (hyper-elastic case). We also note that in the chosen scalings the characteristic length scale is set by the filament cross-section.

By inserting the constitutive relationship for M Equation (7c) in Equation (7b) one obtains explicit differential relationships between the lateral forces and the strains. The tangential component of the force, i.e. f_3, corresponds to the tension (or compression) in the filament and this must be obtained from the condition that d_3 maintains its unit norm. Together with the twist and spin equations (1), one obtains, overall, a system of nine equations (the Kirchhoff equations) for nine unknowns $(f, \kappa, \omega) = (f_1, f_2, f_3, \kappa_1, \kappa_2, \kappa_3, \omega_1, \omega_2, \omega_3)$ which we write in the shorthand form

$$E(f, \kappa, \omega; s, t) = 0. \tag{8}$$

If one fixes a direction in space, the local vectors κ, ω can be expressed in terms of the Euler angles and the system (8) can then be written as a set of 6 equations for 6 unknowns. However, it was shown in [29] that the Euler angles are not always the best choice of variables for studying the stability of stationary solutions. This was illustrated by an analysis of a twisted planar ring: standard statics in the Euler basis yields the well-known result that the critical twist density needed to induce buckling in a ring of radius r is $\gamma_c = \sqrt{3}/r\Gamma$; but calculation of the energy (to third-order) and the action (to fourth-order) did not reveal whether the buckled state is, in fact, the preferred one relative to the initial state. Calculations such as these motivated us to develop a perturbation scheme in terms of the director basis itself.

3. Perturbation Scheme

The basic idea is to expand the director basis associated with the deformed configuration of the filament around the basis of the unperturbed stationary solution, and impose the condition that it remains orthonormal at each order in the perturbation parameter. Namely,

$$d_i = d_i^{(0)} + \varepsilon d_i^{(1)} + \varepsilon^2 d_i^{(2)} + \cdots, \quad i = 1, 2, 3. \tag{9}$$

Applying the orthonormality condition $d_i.d_j = \delta_{ij}$ leads to an expression for the perturbed basis in terms of the unperturbed basis

$$d_i^{(1)} = \sum_{j=1}^{3} A_{ij}^{(1)} d_j^{(0)}, \tag{10a}$$

$$d_i^{(2)} = \sum_{j=1}^{3} \left(A_{ij}^{(2)} + S_{ij}^{(2)} \right) d_j^{(0)}, \tag{10b}$$

$$\vdots$$

$$d_i^{(n)} = \sum_{j=1}^{3} \left(A_{ij}^{(n)} + S_{ij}^{(n)} \right) d_j^{(0)}, \tag{10c}$$

where $A^{(k)}$ is the *antisymmetric* matrix

$$A^{(k)} = \begin{pmatrix} 0 & \alpha_3^{(k)} & -\alpha_2^{(k)} \\ -\alpha_3^{(k)} & 0 & \alpha_1^{(k)} \\ \alpha_2^{(k)} & -\alpha_1^{(k)} & 0 \end{pmatrix}, \tag{11}$$

and $S^{(k)}$ is a *symmetric* matrix whose entries depend only on $\alpha_i^{(j)}$ with $j < k$. For example:

$$S^{(2)} = \begin{pmatrix} -\frac{1}{2}(\alpha_2^{(1)})^2 - \frac{1}{2}(\alpha_3^{(1)})^2 & \frac{1}{2}\alpha_1^{(1)}\alpha_2^{(1)} & \frac{1}{2}\alpha_1^{(1)}\alpha_3^{(1)} \\ \frac{1}{2}\alpha_1^{(1)}\alpha_2^{(1)} & -\frac{1}{2}(\alpha_3^{(1)})^2 - \frac{1}{2}(\alpha_1^{(1)})^2 & \frac{1}{2}\alpha_2^{(1)}\alpha_3^{(1)} \\ \frac{1}{2}\alpha_1^{(1)}\alpha_3^{(1)} & \frac{1}{2}\alpha_2^{(1)}\alpha_3^{(1)} & -\frac{1}{2}(\alpha_1^{(1)})^2 - \frac{1}{2}(\alpha_2^{(1)})^2 \end{pmatrix}. \tag{12}$$

Once the vector $\alpha^{(1)}$ is known the configuration of the perturbed rod is easily reconstructed by integrating the tangent vector:

$$x(s,t) = \int^s \mathrm{d}s(d_3^{(0)} + \varepsilon(\alpha_2^{(1)}d_1^{(0)} - \alpha_1^{(1)}d_2^{(0)})) + O(\varepsilon^2). \tag{13}$$

Since any local vector

$$V = \sum_{i=1}^{3} v_i d_i$$

can be expanded in terms of the perturbed basis; namely $V = V^{(0)} + \varepsilon V^{(1)} + \varepsilon^2 V^{(2)} + \cdots$, we can write a perturbative expansion of the twist and spin matrices, i.e., $K = K^{(0)} + \varepsilon K^{(1)} + \cdots$, $W = W^{(0)} + \varepsilon W^{(1)} + \cdots$, where

$$K^{(1)} = \frac{\partial}{\partial s}A^{(1)} + [A^{(1)}, K^{(0)}], \tag{14a}$$

$$W^{(1)} = \frac{\partial}{\partial t}A^{(1)} + [A^{(1)}, W^{(0)}]. \tag{14b}$$

If needed higher-order terms in the expansion can be generated and easily expressed in terms of the lower-order terms.

Using these equations, one can write the first-order perturbation of the Kirchhoff equations (7a, 7b) in terms of $(\alpha^{(1)}, f^{(1)})$. This system will be referred to as the *dynamical variational equations*. Its solutions control the stability, or lack thereof, of the stationary solutions with respect to linear time-dependent modes. To emphasize the linear character of these equations we rewrite them as a linear system of six equations for the six-dimensional vector $\mu^{(1)} = (\alpha^{(1)}, f^{(1)})$

$$L_E(\kappa^{(0)}, f^{(0)}).\mu^{(1)} = 0, \tag{15}$$

where L_E is a second-order differential operator in s and t whose coefficients depends on s through the unperturbed solution $(\kappa^{(0)}, f^{(0)})$.

4. Linear Stability Analysis

The linear system (15) can be used to determine stability in the standard way: for a given static configuration (characterized by the $(\kappa^{(0)}, f^{(0)})$), stability to linear disturbances is determined by setting the components of μ to be of the form

$$\mu_j = \mathrm{e}^{\sigma t}(Ax_j\,\mathrm{e}^{ins/L} + A^*x_j^*\,\mathrm{e}^{-ins/L}), \quad j = 1, \ldots, 6, \tag{16}$$

where $(\,)^*$ stands for the complex conjugate, n is the mode number, and πL the filament length. (For infinite rods, n/L is replaced by the continuous wave number n.) At the level of the linear theory the amplitude, A, is arbitrary; it can only be determined by proceeding to the nonlinear analysis described in Section 5.

The values of the growth rates σ for which Equation (16) satisfies the variational equations (15), are the ones for which $\Delta = \det(L) = 0$. $\Delta = 0$ defines the *dispersion relation*. This fundamental expression relates the mode number n to the growth rate σ. The technically difficult part of this calculation is computational: the dispersion relations are high-order polynomials in σ and n and can involve many hundreds of terms (for the helix, it is over 500 terms!) and can really only be handled by substantial symbolic manipulation. We note that in all the linear stability analyses we have studied to date, we only consider $\sigma \in \mathbb{R}$. The dispersion relation can have other solutions corresponding to *vibration modes* (i.e. $i\sigma \in \mathbb{R}$). These modes are not spontaneously unstable, i.e. their amplitude is at most of the size of the perturbation itself and they would have to be explicitly excited in order to be observed. Although such oscillatory modes are apparently not relevant to basic stability considerations, they may still play a subtle role in the nonlinear behavior beyond the threshold. This is an interesting open question that we have not yet explored.

4.1. Twisted Planar Ring

We now apply the linear analysis described above to the particular case of the twisted planar ring. We address a classic problem: at what value of the twist, does the planar ring becomes unstable and buckle out of the plane? As we mentioned in Section 2, an analysis based on statics alone does not seem to be able to address this problem completely. The time dependent approach answers this question unambiguously.

The stationary solution for a twisted planar ring is given by

$$\kappa^{(0)} = (k\sin(\gamma s), k\cos(\gamma s), \gamma), \tag{17a}$$

$$f^{(0)} = (\Gamma\gamma k\sin(\gamma s), \Gamma\gamma k\cos(\gamma s), 0), \tag{17b}$$

where k is the inverse of ring radius (from the center to the central ring axis) and $\gamma = k\mathrm{Tw}$ is, effectively, the twist density (here Tw is the total twist in the ring). With this choice of vector κ, the director basis (d_1, d_2) rotates about the central axis with the twist of the rod.

In carrying out the linear analysis some care must be taken with the boundary conditions due to the periodic structure of the ring: these issues are discussed in [30]. In developing the linear variational equations one finds that the α and $f^{(1)}$ are non-autonomous. This is readily dealt with by introducing a linear transformation composed of a reflection about the axis d_1 and a rotation of angle γ about d_3

$$R_\gamma = \begin{pmatrix} \cos(\gamma s) & -\sin(\gamma s) & 0 \\ -\sin(\gamma s) & -\cos(\gamma s) & 0 \\ 0 & 0 & 1 \end{pmatrix}. \tag{18}$$

This transformation is applied to both the basis of the unperturbed system, $d^{(0)}$, and the variables α and $f^{(1)}$. This yields the new variables $\beta = R_\gamma.\alpha$ and $g = R_\gamma.f^{(1)}$, which together make up the components of the vector μ (16).

The net result of the stability analysis is a linear system of equations of the form $L.x + L^*.x^* = 0$, where

$$L = \tag{19}$$

$$\begin{pmatrix}
2ik^3\Gamma\gamma n & \sigma^2 & k^3\Gamma\gamma\left(1+n^2\right) & -k^2\left(1+n^2\right) & 0 & 2\,\mathrm{in}k^2 \\
-\sigma^2 & 0 & 0 & 0 & -n^2k^2 & 0 \\
-k^3\Gamma\gamma\left(1+n^2\right) & 0 & 2\,\mathrm{ik}^3\Gamma\gamma n & -2\,\mathrm{ink}^2 & 0 & -k^2\left(1+n^2\right) \\
-k^2(\Gamma+n^2-1)-\sigma^2 & -\mathrm{ik}\Gamma\gamma n & i\Gamma k^2 n & 0 & 1 & 0 \\
ik\Gamma\gamma n & -n^2k^2-\sigma^2 & k\Gamma\gamma & -1 & 0 & 0 \\
-i\Gamma k^2 n & 0 & -\Gamma n^2k^2-2\sigma^2 & 0 & 0 & 0
\end{pmatrix}.$$

Written out explicitly the dispersion relation takes the form

$$\begin{aligned}
\Delta \;=\; & -2k^2(n^4k^2-2n^2k^2+n^2+1+k^2)(n^2k^2+1)\sigma^6 \\
& -k^4n^2(2\Gamma k^4+2n^4\Gamma k^2-2k^4+\Gamma n^2-10n^4k^4+3\Gamma k^2-3\Gamma k^4n^2-4n^2k^2 \\
& +4n^6k^4+8k^4n^2+\Gamma+\Gamma n^2k^2+4n^4k^2+\Gamma+\Gamma n^2k^2+4n^4k^2+\Gamma n^6k^4)\sigma^4 \\
& -k^8n^4(n-1)(1+n)(2n^4k^2+2n^4\Gamma k^2+2\Gamma n^2-4n^2k^2-2\Gamma^2\gamma^2n^2 \\
& -\Gamma n^2k^2+2\Gamma^2\gamma^2+2k^2-\Gamma k^2)\sigma^2 \\
& -k^{10}\Gamma n^6(n-1)^2(1+n)^2(n^2k^2-\Gamma^2\gamma^2-k^2)
\end{aligned} \tag{20}$$

This relationship, which is an even polynomial of degree 6 in σ and degree 12 in n, captures the essence of the linear stability problem. Solutions with real positive σ identify the unstable modes which grow exponentially out of infinitesimal perturbations; whereas the other modes, which are either oscillatory or exponentially damped, will be of the order of the perturbation itself and, therefore, not observable. A typical plot of σ *versus* n is shown in Figure 1. For large n all modes are seen to be oscillatory.

The dispersion relations determine the critical value of the twist $\mathrm{Tw} = k\gamma$ for which the stationary solution first becomes unstable: this is the value of γ_c for which $\Delta(\sigma = 0) = 0$. It is

$$\mathrm{Tw}_c = \pm\frac{\sqrt{n^2-1}}{\Gamma}. \tag{21}$$

The first mode to become unstable is the mode $n = 2$ with twist $\mathrm{Tw}_c > \sqrt{3}/\,\Gamma$. The evolution of this mode is shown in Figure 2 for growing amplitude up to second-order in ε. Our linear analysis constitutes a direct proof of the twist instability of the ring. Although this condition (21) is well known on the basis of static arguments [1], these arguments cannot prove the actual dynamical instability of the mode after bifurcation. The solution for a given mode can be found by first finding the real positive value of σ such that the nth mode is excited ($\Delta(\sigma) = 0$) and second, by computing the null-space of L corresponding to that value of σ. Having obtained a solution for $\{\beta, g\}$, we can obtain $\alpha = {R_\gamma}^{-1}.\beta$ and $f^{(1)} = {R_\gamma}^{-1}.g$. The solution $X = X^{(0)} + \varepsilon X^{(1)}$ can then be reconstructed by the quadrature

$$X^{(1)} = \int \mathrm{d}s(\alpha_2 d_1^{(0)} - \alpha_1 d_2^{(0)}). \tag{22}$$

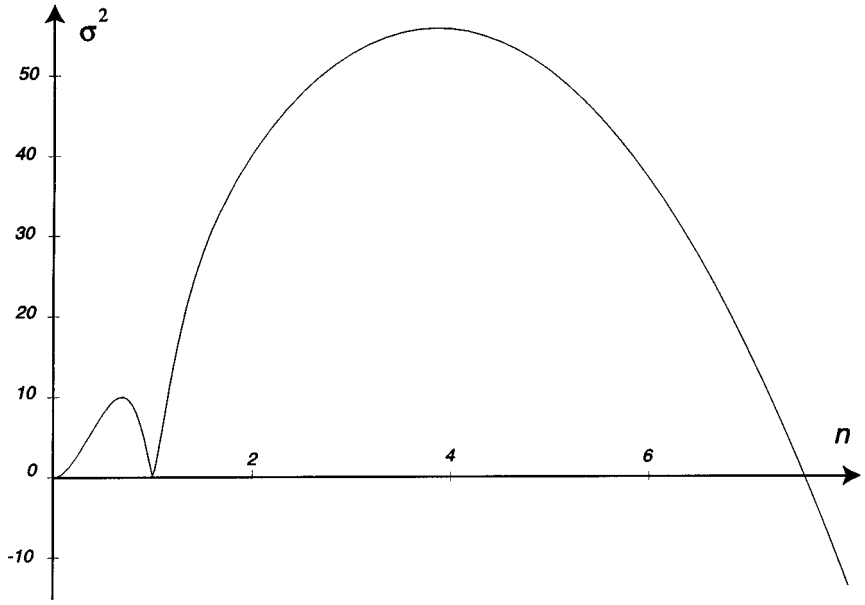

Figure 1. σ^2 as a function of n. The total twist is $\mathrm{Tw} = 30 \gg \mathrm{Tw}_c$.

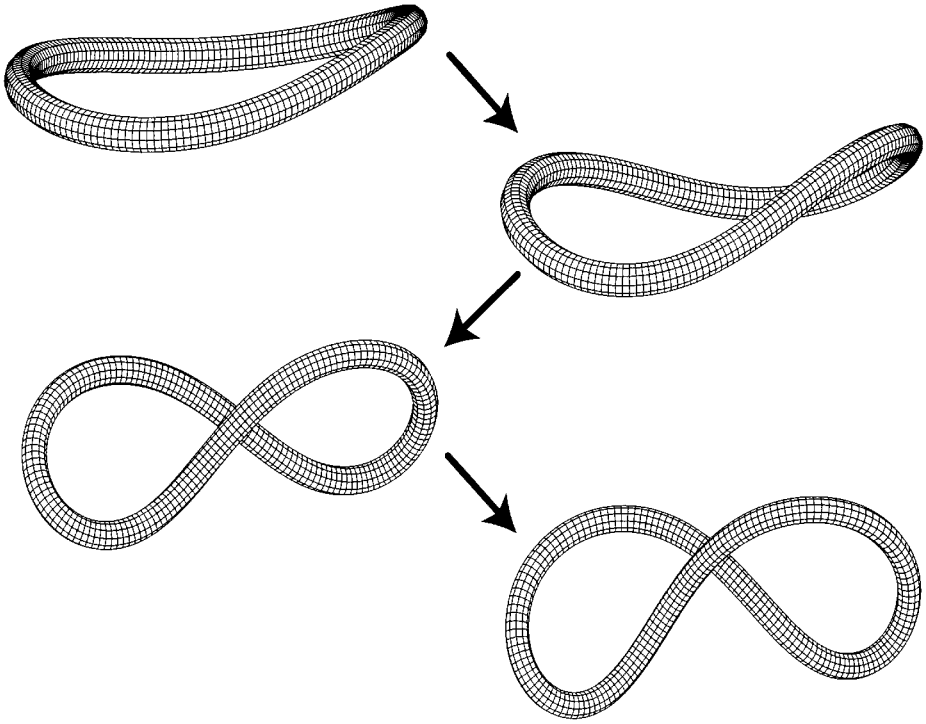

Figure 2. Evolution of the mode $n = 2$ for growing amplitude ($k = 1/16,\ \Gamma = 3/4$).

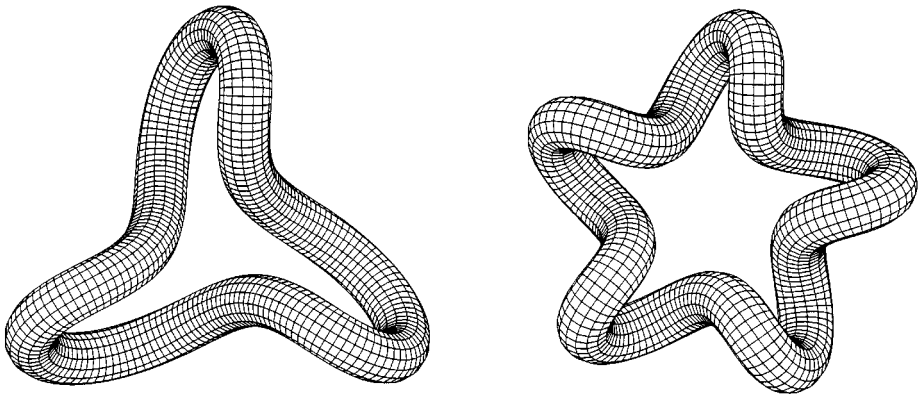

Figure 3. Linear fundamental unstable solution for the modes $n = 3$ and $n = 5$ ($k = 1/16,\ \Gamma = 3/4$).

The explicit form of $X^{(1)}$ is quite complicated so, instead, we show in Figure 3 the different modes $n = 3$ and $n = 5$. These are the fundamental modes which can become unstable as γ increases.

The dispersion relations can also help answer another important question: given that a ring becomes unstable, what is the actual shape that one sees appear? This is the *selection problem*. Numerical simulations [27, 28] show that planar rings twisted well beyond the buckling threshold appear to favor a given geometry as they evolve into the buckled state. The shape selected by the ring at the onset of instability is determined by the unstable initial modes. Since the instability grows exponentially in time, we expect to see the *most unstable* mode grow faster than the others and hence to be the first observed. This dominant mode is simply read off the graph of the dispersion relations. By definition, this mode selection is a dynamical process and cannot be determined from an analysis of the static problem.

We illustrate this by considering the particular case shown in Figure 1. We see that the modes $n = 2$ to $n = 7$ are unstable; however, it is clear that the fastest growing unstable mode is the mode $n = 4$ (The maximum is reached at $n \approx 3.855$). We therefore expect the mode $n = 4$ to be the dominant mode in the dynamics and the ring to select the associated shape. The time evolution of this mode is shown in Figure 4. Here, we are only showing the evolution governed by the linear theory and one should not expect the actual longtime behavior to follow these deformations. However, as mentioned earlier, numerical simulations show that, typically, the growth is dominated by a single mode and that the early stages of evolution are, in fact, rather well modeled by the linear theory.

4.2. Twisted Straight Rod

One of the oldest, and simplest, cases of an elastic instability is that of the straight rod subjected to twist and tension (or compression) [17, 20]. The classical studies are again based on stationary perturbations of static solutions and can only address the most basic stability issues. Here, the full three-dimensional dynamical problem is considered within the framework of Kirchhoff theory.

We consider a straight infinite twisted rod along the x-axis. The twist density in the rod is γ. The stationary solutions is then given by

$$\kappa^{(0)} = (0, 0, \gamma), \tag{23a}$$

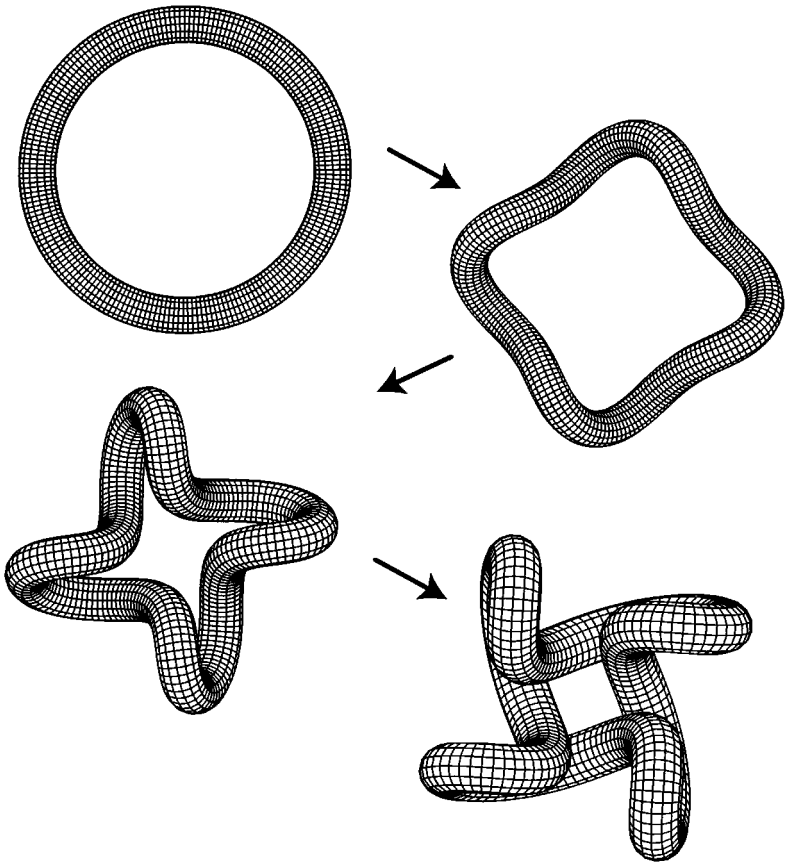

Figure 4. Evolution of the unstable solution for the modes $n = 4$ for $k = 1/16,\ \Gamma = 3/4$.

$$f^{(0)} = (0, 0, P^2). \tag{23b}$$

where P^2 represents the tension/compression along the rod. The interplay between the parameters, P and γ determine the stability characteristics of the rod. To begin with we only consider a rod under tension, i.e., $f_3^{(0)} > 0$; the same analysis applies to a rod under compression.

The linear solutions can be expressed as

$$\alpha_j = \mathrm{e}^{\sigma t}(A x_j \,\mathrm{e}^{ins} + A^* x_j^* \,\mathrm{e}^{-ins}), \quad j = 1, 2, 3, \tag{24a}$$

$$f_j^{(1)} = \mathrm{e}^{\sigma t}(A x_{j+3} \mathrm{e}^{ins} + A^* x_{j+3}^* \,\mathrm{e}^{-ins}), \quad j = 1, 2, 3, \tag{24b}$$

where $\sigma = \sigma(n)$ is a solution of the dispersion relation $\Delta = \Delta(\sigma, n)$. The instability threshold(s) is determined by the *neutral curves*, that is the values of the parameters for which $\sigma = 0$. These curves are given by the solution of $\Delta(0, n) = 0$

$$\Delta(0, n) = (\gamma^2 - n^2)[(\gamma^2(\Gamma - 1) - P^2 - n^2)^2 - \gamma^2(\Gamma - 2)^2 n^2] = 0.$$

The first instability of the rod can now be determined. The solution of the dispersion relation is shown as a function of n for a particular value of P in Figure 5. The relation

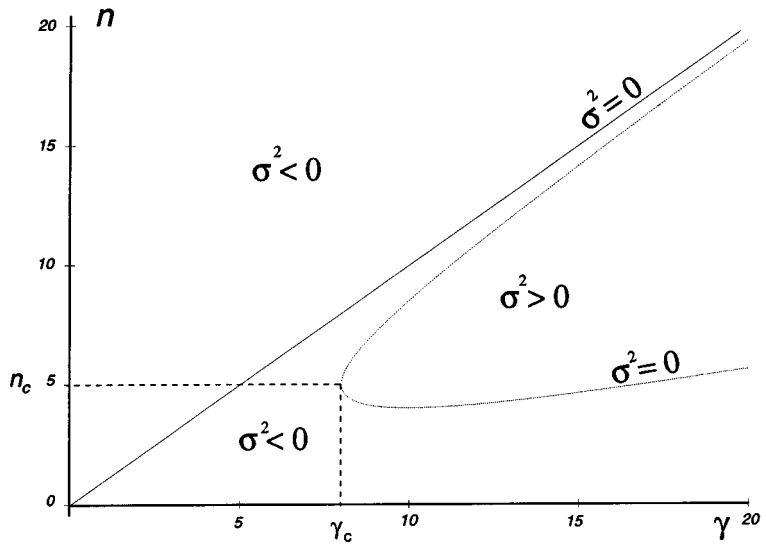

Figure 5. Dispersion relation for $P = 3$, the straight line corresponds to a trivial straight solution curve while the parabola is the neutral curve defining the linearly unstable helical mode.

$\Delta(0, n) = 0$ identifies, to first-order, two different stationary solutions. The first one, corresponding to the straight line on Figure 5, does not correspond to an actual solution (on this curve $\kappa^{(1)} = \omega^{(1)} = 0$ identically). The second solution, corresponding to the parabolic curve in Figure 5, is physically significant and corresponds to a *helical mode*. For this curve the critical values are

$$n_c = \frac{P(2-\Gamma)}{\Gamma}, \quad \gamma_c = \pm 2\frac{P}{\Gamma}. \tag{25}$$

These new solutions take the form (obtained by the integration of Equation 13)

$$X = \left(s, 2\,\frac{A}{P}\cos sP, 2\frac{A}{P}\sin sP \right). \tag{26}$$

Thus for fixed P, the straight rod becomes unstable at the critical twist γ_c and deforms into a helix. Some examples of these helical modes are shown in Figure 6.

We conclude by noting that the above discussion has been limited to infinite rods. The bifurcation condition for rods of finite length exhibits a 'delay' inversely proportional to the square of the rod length, i.e. the shorter the rod the sooner the bifurcation occurs. This will be discussed in the context of the nonlinear analysis described in the next section.

4.3. Helical Rod

One of the most fundamental, naturally occurring, filamentary structures is the helix – which appears in fields ranging from molecular biology to magnetohydrodnamics. Furthermore, helical rods are, subject to appropriate boundary conditions, stationary solutions to the Kirchhoff equations. However, despite their ubiquity, a rather basic question remains unanswered; namely are helical configurations stable to perturbation? In fact the results of the previous section on straight rods makes this question particularly pertinent. If a twisted straight rod bifurcates into a helix, is that mode itself stable, or will it undergo a secondary bifurcation

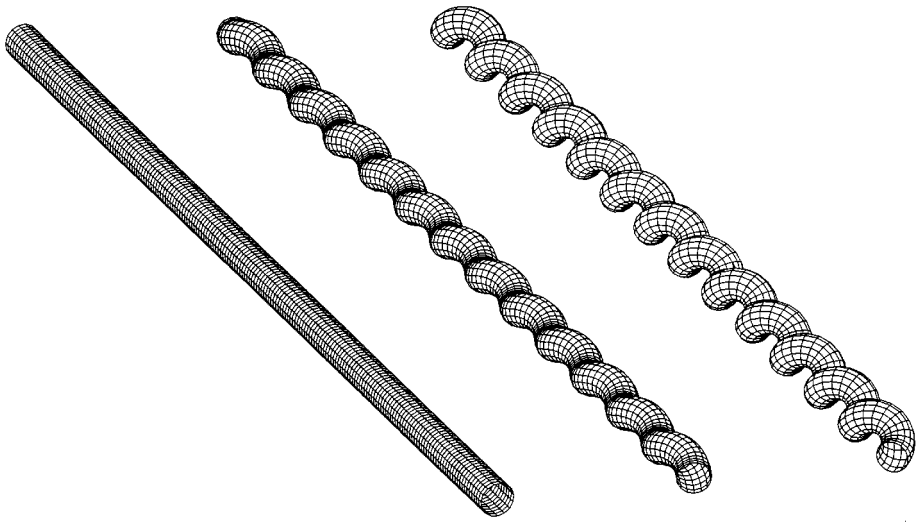

Figure 6. Perturbation of a straight rod for $n_c = 5,\ \gamma_c = 8,\ P = 3$. From left to right $A\varepsilon = 0,\ 0.3,\ 0.6$.

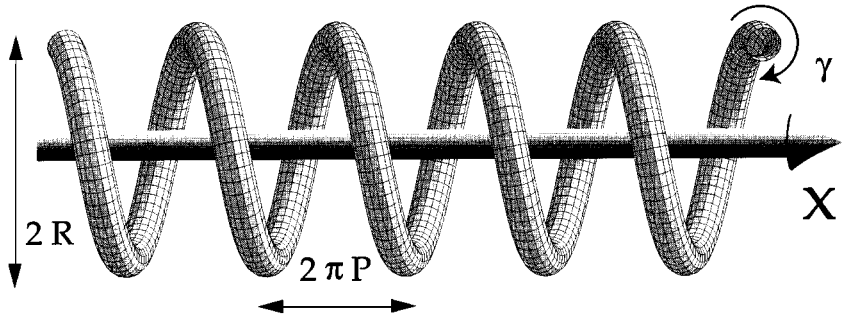

Figure 7. A helical rod characterized by an applied twist γ, a radius R, and a loop-to-loop distance $2\pi P$.

into another configuration? The tools we have developed are able to answer this and other questions about the stability of helical configurations.

Here we consider a helical space curve, x_h, parameterized by arc-length, s, turning around a cylinder of radius R whose central axis points along the x-axis

$$x_h = (P\delta s,\, R\cos(\delta s),\, R\sin(\delta s)), \tag{27}$$

where $\delta = \pm\sqrt{1/(P^2 + R^2)}$. The choice + defines a right-handed helix for $P > 0$ (i.e. if you point your right-hand thumb along the x-axis, your hand will naturally rotate to the right as you move along the helix). The height (along the x-axis) per turn of the helix is $h = 2\pi P$ and the length of the curve per turn is $l = 2\pi/\delta$. Thus,for a helix of N turns, the total height is $H = 2\pi PN$ and the total filament length is $L = 2\pi N/\delta$. A sketch of a helical rod with an applied axial twist is shown in Figure 7.

It is straightforward to construct the Frenet triad for this helix beginning with the tangent vector $\mathrm{T}(s) = x_h'(s)$. One obtains

$$\mathrm{T}(s) \;=\; (P\delta,\, -R\delta\sin(\delta s),\, R\delta\cos(\delta s)), \tag{28a}$$

$$\mathrm{N}(s) \;=\; (0,\, -\cos(\delta s),\, -\sin(\delta s)), \tag{28b}$$

$$\mathrm{B}(s) \;=\; (-R\delta, -P\delta\sin(\delta s),\, P\delta\cos(\delta s)). \tag{28c}$$

The associated Frenet curvature, κ_F, and torsion, τ_F, are

$$\kappa_F \;=\; R\delta^2 = \frac{R}{P^2+R^2}, \tag{29a}$$

$$\tau_F \;=\; P\delta^2 = \frac{P}{P^2+R^2}. \tag{29b}$$

Since we are interested in actual helical rods with axial twist it is convenient to represent this twist by a *ribbon* attached to x_h which twists around the space curve with a given rotation angle $\gamma(s)$. The ribbon construction naturally introduces the director basis

$$d_1^{(0)} \;=\; \cos(\gamma s)\mathrm{N} - \sin(\gamma s)\mathrm{B}, \tag{30a}$$

$$d_2^{(0)} \;=\; -\sin(\gamma s)\mathrm{N} - \cos(\gamma s)\mathrm{B}, \tag{30b}$$

$$d_3^{(0)} \;=\; \mathrm{T}, \tag{30c}$$

which is simply a rotation of the Frenet triad in the plane normal to T.

The twist vector may now be computed by substituting the new triad into the twist equation (1a) and solving for the unknowns $\kappa^{(0)}$. This yields

$$\kappa^{(0)} = (\kappa_F\sin(\gamma s), \kappa_F\cos(\gamma s), \tau_F + \gamma), \tag{31}$$

where γ is the twist density of the rod.

So far our discussion of the helix has been purely geometrical. To determine the physical forces acting on our rod – assumed for now to be in a static configuration – we need to solve the time independent Kirchhoff equations. Despite the relative simplicity of this calculation, a number of interesting results follow. For greatest generality in the constitutive relations (5) we choose the intrinsic curvature components, κ^u to correspond to another helix, i.e.

$$\kappa^u = (\kappa_F^u\sin(\gamma^u s), \kappa_F^u\cos(\gamma^u s), \tau_F^u + \gamma^u), \tag{32}$$

where κ_F^u, τ_F^u, R^u, and P^u are, respectively, the Frenet curvature, Frenet torsion, radius, and pitch associated with this helix and γ^u is a specified twist density. Thus the 'natural' state of our rod is a helix with the above specified parameters. Although we have specified an additional twist density γ^u it is easily demonstrated that static solutions for the helix only exist when the stressed and unstressed twist densities are the same, i.e., $\gamma = \gamma^u$. However, these need not be equal in the special limiting case of a helix of zero radius, i.e. a straight rod.

Given $\kappa^{(0)}$ and κ^u it is then straightforward to solve the Kirchhoff equations to determine the force components. These are

$$f^{(0)} = \left(f_0\sin(\gamma s),\, f_0\cos(\gamma s),\, \frac{\tau_F}{\kappa_F}f_0\right), \tag{33}$$

where

$$f_0 = -\tau_F(\kappa_F - \kappa_F^u) + \Gamma\kappa_F(\tau_F - \tau_F^u) \tag{34}$$

and we are assuming that $\kappa_F \neq 0$.

To hold a helix in a given shape, it is usually necessary to apply a terminal force, i.e. a force f_x, pointing along the x-axis and applied at the ends of the rod. One may show that $f_x = f_0 \sec(\alpha)$, where α is the pitch angle defined as $\tan(\alpha) = R/P$. It is clearly possible to construct a 'free standing' helix, namely one for which no terminal forces are required, corresponding to the condition $f_0 = 0$. Thus, for example, if the unstressed configuration is a naturally straight rod, (i.e. $\kappa_F^u = 0$), the free standing condition is $\gamma = \tau_F(1-\Gamma)/\Gamma$. However, it is important to note that even if terminal forces are not required, a terminal moment has to be applied to maintain the helical structure.

A linear stability analysis of the stationary helix can now be performed exactly as before; and as in the case of the ring an additional transformation of the form (18) is required to make the linearized equations autonomous. The actual computations are very long and rely heavily on symbolic manipulation. The dispersion relations are extremely complicated and are generally not written out explicitly. However, given the growth rate for an unstable mode with mode number n, the explicit form of the excited state takes the general form

$$\begin{aligned}
x_1(s,t) &= P\delta s - \frac{2NKR\xi_1}{n\tau_F}\cos\left(\frac{n\delta s}{N}\right),\\
x_2(s,t) &= R\cos(\delta s) - \frac{K}{\delta}\left[\frac{\xi_2-\xi_1}{n-N}\sin\left(\frac{n-N}{N}\delta s\right) + \frac{\xi_2+\xi_1}{n+N}\sin\left(\frac{n+N}{N}\delta s\right)\right],\\
x_3(s,t) &= R\sin(\delta s) - \frac{K}{\delta}\left[\frac{\xi_2-\xi_1}{n-N}\cos\left(\frac{n-N}{N}\delta s\right) - \frac{\xi_2+\xi_1}{n+N}\cos\left(\frac{n+N}{N}\delta s\right)\right],
\end{aligned}$$

where $K = \varepsilon C\,\mathrm{e}^{\sigma t}$ and ξ_1 and ξ_2 are complicated functions of $\sigma, n, N, \delta, \Gamma, \kappa_F, \kappa_F^u, \tau_F, \tau_F^u$. Their explicit form is given in [32].

Obviously in considering the stability of a helix there are many choices of parameters: the geometric parameters, the intrinsic properties, and the elastic constant. For illustrative purposes we summarize the results for the simplest case: namely a helix constructed from a naturally straight and untwisted rod, i.e. one for which $\kappa^u = (0,0,0)$ and $\gamma = 0$. A detailed discussion of this case as well as the behavior of intrinsically curved and twisted helices is given in [32]. Analysis of the dispersion relation for our chosen problem reveals that there are three neutral modes

$$\left(\frac{n}{N}\right)^2 = 0, \quad \left(\frac{n}{N}\right)^2 = 1, \tag{35a}$$

$$\left(\frac{n}{N}\right)^2 = ((\Gamma-2)^2\tau_F^2 + \kappa_F^2\delta^{-2} > 1. \tag{35b}$$

The behavior of σ around threshold can be estimated by a local expansion. Thus around $n/N = 1$, an expansion in powers of n gives

$$\sigma^2 = (1-\Gamma)\delta^4\left(\frac{n}{N}-1\right)^2 + \mathrm{O}\left(\left(\frac{n}{N}-1\right)^4\right). \tag{36}$$

Since there is no neutral mode between $n/N = 0$ and $n/N = 1$ and locally $\sigma > 0$ around $n = 1$, we conclude that $\sigma_n > 0$ for all modes between $n = 1$ and $n = N-1$ and hence that all these modes are unstable. A typical plot of the dispersion relation is shown in Figure 8.

We are now able to answer a basic selection problem: if a naturally straight rod is maintained in a helical shape and suddenly released, toward what shape will it evolve? Since all

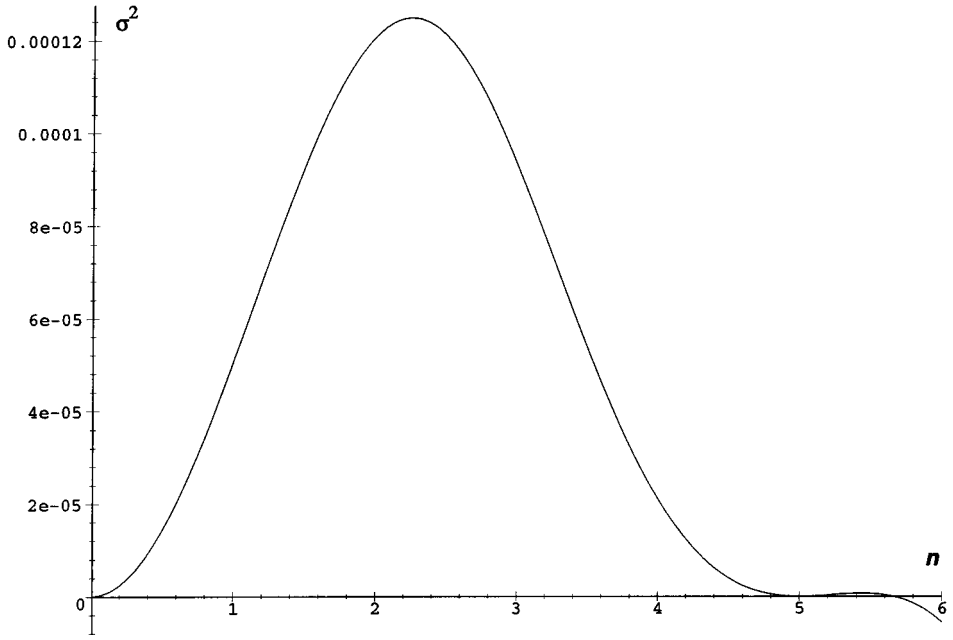

Figure 8. The growth rate σ^2 solution of the dispersion relation for the (naturally straight) helical rod as a function of the spatial mode n. The maximum is obtained close to $n = 2$ ($\kappa_F = 1/8$, $\tau_F = 1/8$, $N = 5$).

the modes from $n = 1$ to $N - 1$ are unstable and if the helix has more than one turn (i.e. $N > 1$), the helix will be unstable. The evolution will be dominated by the fastest growing mode which, for the parameters considered here, can be read off Figure 8; namely the mode $n = 2$. The evolving state (at the level of the linear analysis) is shown in Figure 9. What is quite striking is that instability tends to localize the deformation at two points in a way that is characteristic of buckling behavior.

In addition to the case just described we have also studied the behavior of helical filaments with non-zero intrinsic curvature and find that they are typically dynamically stable. Another situation of interest is to consider the case of free standing helices subject to pulling or pushing. Typically when such a helix is pushed, the resulting instability correspond to a bending of the entire helix, much like the bending of a straight rod. The unstable modes are located around the principal neutral mode $n = N$, so that the instability occurs at the scale of the helix itself. By contrast when the helix is pulled and twisted, a *higher* mode n_c is excited and the helix deforms throughout the rod by creating $n_c > N$ loops along the helix. This latter case should be contrasted with the case where the external parameters are held fixed but the intrinsic curvature is changed. Then, the helix undergoes unstable deformations by exciting *lower* modes $n_c < N$. This leads to the possibility of buckle formation as shown in Figure 9. It is this observation that provides the motivation for the dynamical model of buckling described in Section 6.

5. Nonlinear Analysis

Although the linear analysis identifies the initial instabilities as a function of the parameters and gives the growth rate of the new solutions, it is limited in many respects. Most importantly,

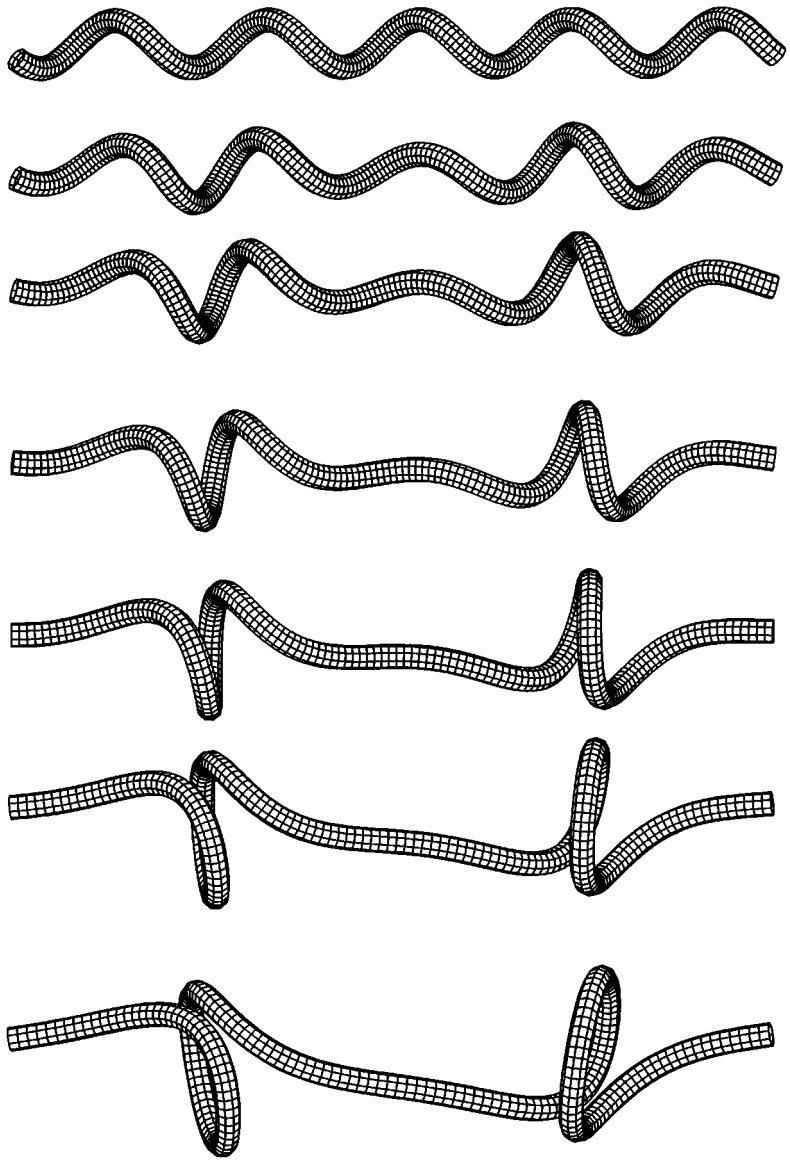

Figure 9. The time evolution of an unstable (naturally straight) helix. The linear mode $n = 2$ creates two loops ($\kappa_F = 1/8$, $\tau_F = 1/8$, $N = 5$ and $K/1000 = 0, 2, 4, 6, 8, 10, 12$). This linear mode might not represent the true evolution of the nonlinear equations and is *a priori* only valid for small values of K (see Section 5).

it is only valid for short times: the exponential growth of the linearized solutions leads to a breakdown of the assumption that these solutions are of order $O(\varepsilon)$ and, furthermore, violates our assumption that the system, which is conservative, is bounded in space and time. Thus as the linear solution grows, the nonlinear terms, neglected in the linear approximation, have to be taken into account.

The main idea behind the nonlinear analysis is to develop an asymptotic expansion of the solution amplitudes, as a function of longer space and time scales, close to the bifurcation point [38]. In this regime, the distance from the bifurcation point is of the order of the perturb-

ation itself. This relationship can then be used to introduce new scales on which the arbitrary linear amplitudes can vary. Here we consider the case of a twisted ring, and then the straight twisted rod. In both cases, we take the twist, γ, as the control (or 'stress') parameter.

5.1. Nonlinear Analysis of the Ring

The unstable modes of the ring are discretized due to the boundary conditions and the shape of the neutral dispersion curves around the origin. Therefore, a nonlinear analysis can only take into account the temporal evolution of discrete modes. For twist value greater but close to the critical twist, there is only one unstable mode, namely $n = 2$ (see Figures 1 and 2). Thus, we seek to derive an equation describing the temporal evolution of its amplitude A and drop all possible dependence on longer space scales. If the system is close enough to the bifurcation, the difference between the twist density and the critical twist γ_c is proportional to the perturbation parameter itself, namely

$$\varepsilon^2 = \gamma_c - \gamma. \tag{37}$$

The new, longer, time scale is $t_1 = \varepsilon t$. The choice of this new scale can be justified by expanding the dispersion relation in power of ε (see [31]). Taking into account the possibility of the solutions varying on this new (independent) scale, one can now solve the hierarchy of systems obtained by expanding all dependent variables in terms of ε

$$0(\varepsilon^0): \quad E(\mu^{(0)}; s_0, t_0) = 0, \tag{38a}$$

$$0(\varepsilon^1): \quad L_E(\mu^{(0)}; s_0, t_0).\mu^{(1)} = 0, \tag{38b}$$

$$0(\varepsilon^2): \quad L_E(\mu^{(0)}; s_0, t_0).\mu^{(2)} = H_2(\mu^{(1)}), \tag{38c}$$

$$0(\varepsilon^3): \quad L_E(\mu^{(0)}; s_0, t_0).\mu^{(3)} = H_3(\mu^{(1)}, \mu^{(2)}), \tag{38d}$$

$$\vdots$$

where H_i is polynomial in its arguments and derivatives in s_0, t_0, t_1.

To first-order one obtains the linear solution

$$\mu^{(1)} = C_0\xi_0 + A(t_1)\,\xi_2\,\mathrm{e}^{i(2s/k)} + \text{c.c.}, \tag{39}$$

where c.c. stands for the complex conjugate of the previous expression, $\xi_0, \xi_2 \in \mathbb{C}^6$ are specified such that $\xi_0.\xi_0 = \xi_2.\xi_2 = 1$ and C_0 is set such that the ring remains closed when it deforms.

The second-order solution can be found in the same way by solving (38c)

$$\mu^{(2)} = \chi_0 + \chi_2\,\mathrm{e}^{i(2s/k)} + \chi_4\,\mathrm{e}^{2i(4s/k)} + \text{c.c.} \tag{40}$$

In order to find a condition on the amplitude $A(t_1)$ we demand that the solutions to the third-order system (38d) remain bounded. Thus, we apply the Fredholm alternative to the system (38d): here this consists of integrating H_3 against all neutral solutions of the adjoint operator $L_E^\dagger$

$$\int_0^L \zeta_1.H_3(\mu^{(0)}, \mu^{(1)}, \mu^{(2)})\,\mathrm{d}s = 0, \tag{41}$$

where $\zeta_1$is the adjoint solution to $\mu_1^{(1)}$ (i.e. $L_E^{\dagger}.\zeta_1 = 0$). This compatibility condition gives rise to a differential equation for A as a function of t_1, which can be written in terms of t

$$\frac{\partial^2 A}{\partial t_1^2} = \frac{A}{27k^2 + 8}\left(24\sqrt{3}\varepsilon^2 k^3 - 6(8\Gamma - 11)|A|^2\right). \tag{42}$$

This equation describes the time evolution of the mode $n = 2$ after bifurcation. An interesting and important consequence that can be read off directly from the equation is that supercritical solutions ($\gamma > \gamma_c$) are *always* unstable unless $\Gamma > 11/8$. In such case, there exist a stationary solutions with amplitude

$$|A|^2 = \frac{4\sqrt{3}\varepsilon^2 k^3}{8\Gamma - 11}. \tag{43}$$

Two comments are in order here, first this result is consistent with a result previously obtained by Maddocks and Rogers [39] on the basis of the static Kirchhoff equations. Second, this result does not seem very useful since the derivation of the Kirchhoff equations from three-dimensional elasticity implies that $2/3 < \Gamma < 1 < 11/8$. However, an argument can be made to show that rods with non-circular cross-sections with high intrinsic twist may actually obey the Kirchhoff equations for circular rods but with $\Gamma > 1$ [40]. Such systems could then exhibit behavior like the one outlined here. Moreover, it seems that the experimental measurements of the ratio between bending and twist coefficients for biological molecules such as DNA strands) are also such that $0.7 < \Gamma < 1.5$ [18]. Such high values of Γ might, on the one hand, justify the applicability of the calculations performed here but, on the other hand, may raise doubts on the general applicability of the Kirchhoff equations to model biological fibers. We believe that this issue is of fundamental importance and should be further studied.

5.2. The Twisted Straight Rod under Tension

We now perform the nonlinear analysis on the twisted straight rod. The main difference here is that the amplitudes of the nonlinear modes can now vary on longer *space scales*. Here again, we can set

$$\varepsilon^2 = \gamma - \gamma_c \tag{44}$$

and introduce the stretched time and space scales

$$t_0 = t, \quad t_1 = \varepsilon t, \tag{45}$$

$$s_0 = s, \quad s_1 = \varepsilon s. \tag{46}$$

Taking into account the expansion in the bifurcation parameter and the new scales, we now look for solutions of the full system order by order in ε

$$0(\varepsilon^0): \quad E(\mu^{(0)}; s_0, t_0) = 0, \tag{47a}$$

$$0(\varepsilon^1): \quad L_E(\mu^{(0)}; s_0, t_0).\mu^{(1)} = 0, \tag{47b}$$

$$0(\varepsilon^2): \quad L_E(\mu^{(0)}; s_0, t_0).\mu^{(2)} = H_2(\mu^{(1)}), \tag{47c}$$

$$0(\varepsilon^3): \quad L_E(\mu^{(0)}; s_0, t_0).\mu^{(3)} = H_3(\mu^{(1)}, \mu^{(2)}), \tag{47d}$$

$$\vdots$$

where now H_i is polynomial in its arguments and derivatives in s_0, s_1, t_0, t_1.

To order $0(\varepsilon)$, the (linear) solution is given by a superposition of the neutral modes; namely

$$\mu^{(1)} = X_0(s_1, t_1)\xi_0 + X_n(s_1, t_1)\xi_n \, \mathrm{e}^{i(ns_0/L)} + X_n^*(s_1, t_1)\xi_n^* \, \mathrm{e}^{-i(ns_0/L)}, \tag{48}$$

where $X_0(s_1, t_1)$ and $X_n(s_1, t_1)$ represent, respectively, the slowly varying amplitudes of the axial twist and the unstable helical mode; $n = n_c$; and

$$\begin{aligned} \xi_0 &= (0, 0, 0, 0, 0, 1), \\ \xi_n &= (1, -i, 0, iP^2, P^2, 0). \end{aligned} \tag{49}$$

At this order of ε the functions X_0 and X_n are arbitrary and are constant on the scales (s_0, t_0) but may vary on the longer scales (s_1, t_1).

In order to derive an amplitude equation describing the evolution of the amplitudes on these new scales we consider the higher-order equations in (47) and look for conditions on the amplitude to ensure that the solution remains bounded. This condition is again found at $O(\varepsilon^3)$ by applying the Fredholm alternative. This calculation shows that the amplitudes $X_0 \equiv Y$, $X_n \equiv X$, must satisfy the following system of equations

$$\left(\frac{P^2+1}{P^2}\right)\frac{\partial^2 X}{\partial t_1^2} - \frac{\partial^2 X}{\partial s_1^2} = P\Gamma X\left(1 - 2P|X|^2 - \frac{\partial Y}{\partial s_1}\right), \tag{50a}$$

$$\frac{2}{\Gamma}\frac{\partial^2 Y}{\partial t_1^2} - \frac{\partial^2 Y}{\partial s_1^2} = 2P\frac{\partial |X|^2}{\partial s_1}. \tag{50b}$$

These equations, which are of the form of a system of two coupled nonlinear Klein–Gordon equations, couple the local deformation of the rod X with the twist density Y. We note the central role played by the twist density in these equation: if we set $Y = 0$, it is easy to see that the stationary solutions may blow up.

The space curve can be reconstructed by integrating the tangent vector up to second-order in the perturbation parameter

$$x(s,t) = \begin{pmatrix} \int (1 - |X|^2)\, \mathrm{d}x \\ \int [\cos(Px)(\mathcal{R}e(X)\, Y - 2\, \mathcal{I}m(X)) - \sin(Px)(\mathcal{I}m(X)\, Y + 2\, \mathcal{R}e(X))]\, \mathrm{d}x \\ \int [\sin(Px)(\mathcal{R}e(X)\, Y - 2\, \mathcal{I}m(X)) - \cos(Px)(\mathcal{I}m(X)\, Y + 2\, \mathcal{R}e(X))]\, \mathrm{d}x \end{pmatrix}. \tag{51}$$

The amplitude equations (50) derive from a Hamiltonian [41]

$$\begin{aligned} \mathcal{H} = \int \Bigg[& \frac{P^2}{P^2+1}\left|\frac{\partial X}{\partial s_1}\right|^2 + \frac{\Gamma P^4}{P^2+1}|X|^4 - \frac{\Gamma P^3}{P^2+1}|X|^2\left(\frac{\partial Y}{1 - \partial s_1}\right) + \left|\frac{\partial X}{\partial t_1}\right|^2 \\ & + \frac{\Gamma P^2}{4(P^2+1)}\left(1 - \frac{\partial Y}{\partial s_1}\right)^2 + \frac{P^2}{2(P^2+1)}\left(\frac{\partial Y}{\partial t_1}\right)^2 \Bigg]\, \mathrm{d}s_1 \end{aligned}$$

such that

$$\frac{\partial^2 X}{\partial t_1^2} = -\frac{\delta \mathcal{H}}{\delta \bar{X}} \quad \frac{\partial^2 Y}{\partial t_1^2} = -\frac{\delta \mathcal{H}}{\delta Y}, \tag{52}$$

where δ refers to the Fréchet derivative.

However, Equations (50) are probably non-integrable (they fail the Painlevé test [42] for partial differential equations). Nevertheless, they admit some interesting special solutions

- *Homogeneous solutions*. The spatially independent form of (50) is simply

$$\frac{\partial^2 X}{\partial t_1^2} = \frac{P^3\Gamma}{P^2+1} X\left(1 - 2P|X|^2\right), \tag{53}$$

where the twist density decouples from the deformation and is set equal to a constant. After integration, the filament solution is found to correspond to a helix

$$x = \left(s, -\frac{2\varepsilon X(\varepsilon t)}{P}\sin sP, \frac{2\varepsilon X(\varepsilon t)}{P}\cos sP\right). \tag{54}$$

- *Periodic solutions*. These solutions are remarkably simple

$$X = \sqrt{\frac{\kappa}{P}}\sin\left(\frac{n\pi s_1}{L}\right),$$

$$Y = -\frac{\kappa L}{2n\pi}\sin\left(\frac{2n\pi}{L}s_1\right),$$

where $\kappa = 1 - (n^2\pi^2)/(P\Gamma L^2)$. If we hold the extremities of a finite rod of length L fixed, the constants K_i are determined and we find an envelope solution for the rod:

$$x(s) = \left(s, \frac{\sqrt{4L^2\varepsilon^2 P\Gamma - 1}}{2PL\sqrt{\Gamma}a_+a_-}(a_-\cos a_+ s - a_+\cos a_- s,\right.$$

$$\left.\frac{\sqrt{4L^2\varepsilon^2 P\Gamma - 1}}{2PL\sqrt{\Gamma}a_+a_-}(a_-\sin a_+ s - a_+\sin a_- s)\right),$$

where $a_\pm = P \pm 1/2L$. This solution is shown in Figure 10 for a particular set of parameters.

This solution shows a delay in the bifurcation as a function of the rod length: the bifurcation now occurs at

$$\gamma = \gamma_c + \frac{1}{4P\Gamma L^2}.$$

A gratifying connection between this result and a classical result is worthy of mention. The stability of a finite straight rod subject to twist and tension or compression was studied long ago at the level of statics [20]. For constant twist, γ, the static equations are linear and it is possible to show that the bifurcation threshold is given by

$$\gamma^2 \geq \frac{4P^2}{\Gamma^2}\left(\frac{1}{4L^2P^2} + 1\right). \tag{55}$$

(Here our rod length is scaled by a factor 2π compared to the formula given in [20].) Taking the square root of both sides and expanding the square root on the right-hand side to first-order, gives

$$\gamma \geq \frac{2P}{\Gamma} + \frac{1}{4L^2\Gamma P}. \tag{56}$$

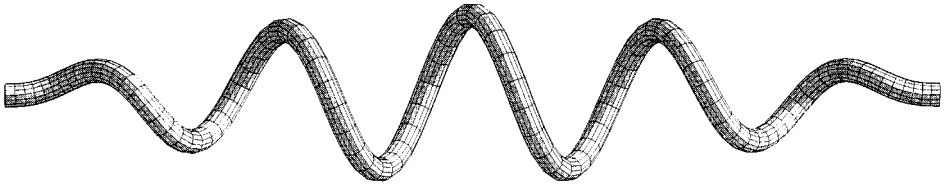

Figure 10. The stationary solution for ($P = 5$, $\Gamma = 3/4$).

This is exactly our 'delay of bifurcation' result deduced from the weakly nonlinear analysis.

- *Traveling pulses*. These solutions can be obtained from the reduction $X = u(s_1 - ct_1)\,\mathrm{e}^{i\theta t_1}$, $Y = v(s_1 - ct_1)$

$$X = \alpha\frac{\sqrt{P^2+1}}{2LP^2}\,\mathrm{sech}\left[\frac{\beta}{L}\left(s_1 - c\sqrt{\frac{\Gamma}{2}}t_1\right)\right]\exp\left[i\left(\frac{k}{L}\left(s_1 - c\sqrt{\frac{\Gamma}{2}}t_1\right) + \frac{\omega}{L}\sqrt{\frac{\Gamma}{2}}t_1\right)\right],$$

$$Y = \frac{\alpha^2}{\beta(c^2-1)}\frac{P^2+1}{2LP^3}\,\tanh\left[\frac{\beta}{L}\left(s_1 - c\sqrt{\frac{\Gamma}{2}}t_1\right)\right],$$

where ω and c are two free parameters and

$$\alpha^2 = \frac{2(c^2-1)}{c^2(c^2-c_0^2)}(\mu(c^2-c_0^2) - \omega^2 c_0^2), \quad \beta^2 = \frac{\mu(c^2-c_0^2) - \omega^2 c_0^2}{(c^2-c_0^2)^2},$$

$$c_0^2 = \frac{2}{\Gamma}\frac{P^2}{P^2+1}, \quad \mu = \frac{2P^3L^2}{P^2+1}, \quad k = \frac{c\,\omega}{c^2-c_0^2}$$

which corresponds to a *pulse-like* solitary wave solutions traveling along the rod with constant speed c. The possible speed intervals for which a traveling pulse exists are given by the condition $\alpha, \beta \in \mathbb{R}$. For instance, in the case $\omega = 0$, we remark that the minimum speed of these traveling waves is $c^2 = \Gamma/2$. This is the speed of the torsional waves obtained from elementary linear elastic theory [21]. We believe that the solutions obtained here are the nonlinear version of torsional waves that takes into account the three-dimensional structure of the system and allow propagation of waves between regions with different twist densities.

- *Front*. The simplest from of the front can be obtained by setting $\theta = 0$ in the previous reduction and considering the case where $P^2/(P^2+1) > c^2 > \Gamma/2$. One can then find a heteroclinic connection of the form

$$X(z) = \alpha\tanh(\beta z), \tag{57}$$

with $\alpha^2 = 1/(2P)$ and $\beta^2 = c^2P^3\Gamma/((P^2c^2 - P^2 + c^2)(\Gamma - 2c^2))$, which describes a *front-like* solitary waves connecting two different asymptotic states. The two different solutions (pulses and front) are shown on Figure 11.

The amplitude equations (50) are of interest in their own right and have recently been the subject of more theoretical and numerical study [41]. In particular, the stability of the particular solutions has been investigated and a whole new 2-parameter family of particular closed-form solutions has been discovered. This family contains among other, homogeneous solutions, traveling pulses, fronts and traveling holes (also called gray solitons).

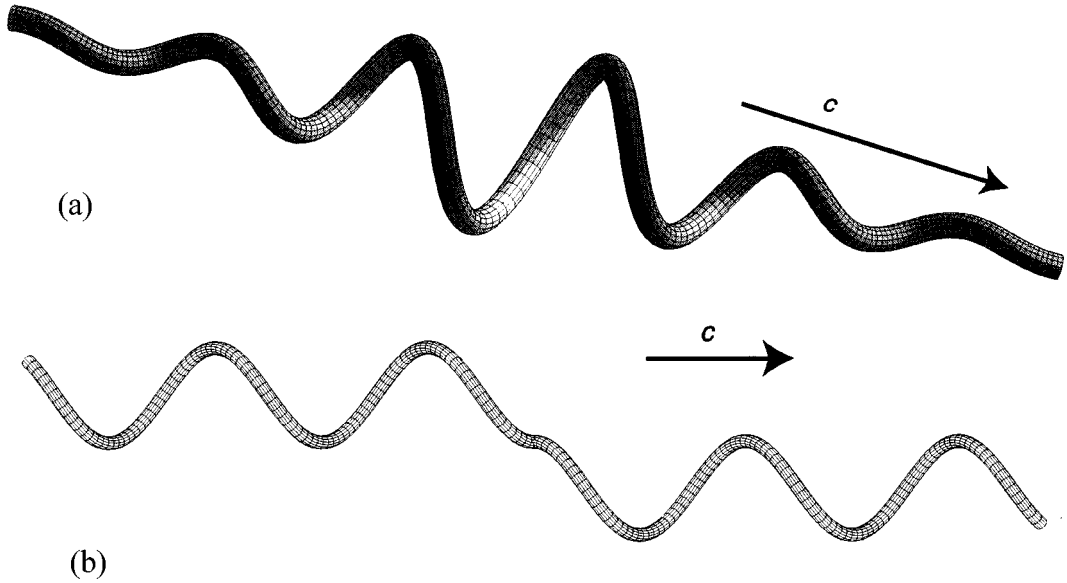

Figure 11. Traveling waves solutions: (a) the pulse ($c = 4$, $P = 7$ and $\omega = 0$) and (b) front solutions ($c = 0.7$, $P = 1$). $\Gamma = 3/4$ in both cases.

6. Dynamical Model of Buckling

It is easily demonstrated that as a small amount of twist is injected into a straight rod, it deforms into a helical form (with very small radius) which, as the twist is further increased, tends to localize in the middle of the rod and eventually forms a loop. Experimental studies of filament twisting [17] have shown that this sequence of bifurcations is qualitatively correct. Here we draw together the results of the previous sections to develop a *dynamical* model of buckling in which this process is characterized as a sequence of bifurcations of the solutions to the Kirchhoff equations in which the twist density is taken as a control parameter. The sequence of bifurcations that constitutes our model of spontaneous looping can be summarized as follows.

6.1. Primary Bifurcation

(a) A straight rod, with arbitrary twist, γ_S, and tension P^2, is shown to become linearly unstable at a critical twist value $\gamma_S = \gamma_1$ (for a given P) and then bifurcate into a helix. The description at this stage of the process involves a direct application of the linear stability analysis of the straight rod given in Section 4.

(b) The geometry of the helical solution, i.e. its pitch and radius, is completely specified by using nonlinear analysis to determine its amplitude. Here we are able to use the results of the nonlinear analysis in Section 6 and the properties of the amplitude equation (50).

(c) The redistribution of the original straight rod twist, γ_S, into the twist, γ_H, and torsion, τ_F, of the new helix is determined using energy considerations. The helix can now be specified by its curvature κ_F, τ_F, and γ_H.

6.2. Secondary Bifurcation

(a) Since the helix itself is an exact solution of the Kirchhoff equations, its linear stability can also be analyzed (again by direct application of the results in Section 4) and the critical twist value, $\gamma_H = \gamma_2$, at which it becomes unstable is determined.

(b) The (linear) post-bifurcation solutions are constructed and a solution with one loop (such as the one shown on Figure 12d), of arbitrary amplitude, B, is identified.

(c) A nonlinear analysis of the unstable helical mode found in step (b) is used to determine the amplitude, B, of the loop. Here a one mode amplitude equation (analogous to the one determined for the ring) is obtained of the form

$$\frac{\partial^2 B}{\partial t_1^2} = B(c_1 - c_3|B|^2), \tag{58}$$

where c_1 and c_3 are extremely complicated algebraic functions of the system parameters whose explicit form is given in [33]. Since all the parameters involved in the coefficients of the amplitude equation depend on the control parameter γ_S, the stationary solution of (58), i.e. $B^2_{\text{stat}} = c_1/c_3$, gives an explicit relationship between the amplitude and the initial twist density.

6.3. Tertiary Bifurcation

(a) A simple criterion to determine the critical B value, B_c, at which the loop will flip is developed following the work of Coyne [2].

(b) The twist value, γ_3, at which the loop amplitude equals B_c is found using the properties of the solution to Equation (58).

The various special values of the twist, $\gamma_H, \gamma_2, \gamma_3$, can all be related back to the initial twist density, γ_S, injected into the straight rod. Thus, in the entire sequence of events γ_S can be considered as the 'control' parameter and its critical values at each stage determined explicitly. A sequence of rod configurations as a function of increasing γ values is shown in Figure 12.

Overall, this multistep dynamical model appears to be consistent with experimental observations, with the possible exception of the very first step. Here we note that in the experimental work of Champneys and Thompson [17], the initial helical solution just described (corresponding, in their terminology, to the classic H_3 solution), is not actually observed. They find that under rigid loading conditions a helical deformation consisting of one twist per wave (the state H_1) can often appear as a result of continuous deformation i.e. as a pre-bifurcation phenomenon. Rather than observe the three twists per wave helical solution, H_3, they see a localized helical structure L_3 (which also has approximately three twists per wave). It is this state that then undergoes a writhing instability into the looped state. The main difference between their experimental observations and our theoretical model is that we do not observe the H_1 state. However, this is not too surprising since subsequent studies by Champneys et al. [43] show that the appearance of this solution results from the influence of a small initial curvature in the rod – an effect not included in our model. Beyond this, their observations and the rest of our model are consistent with each other.

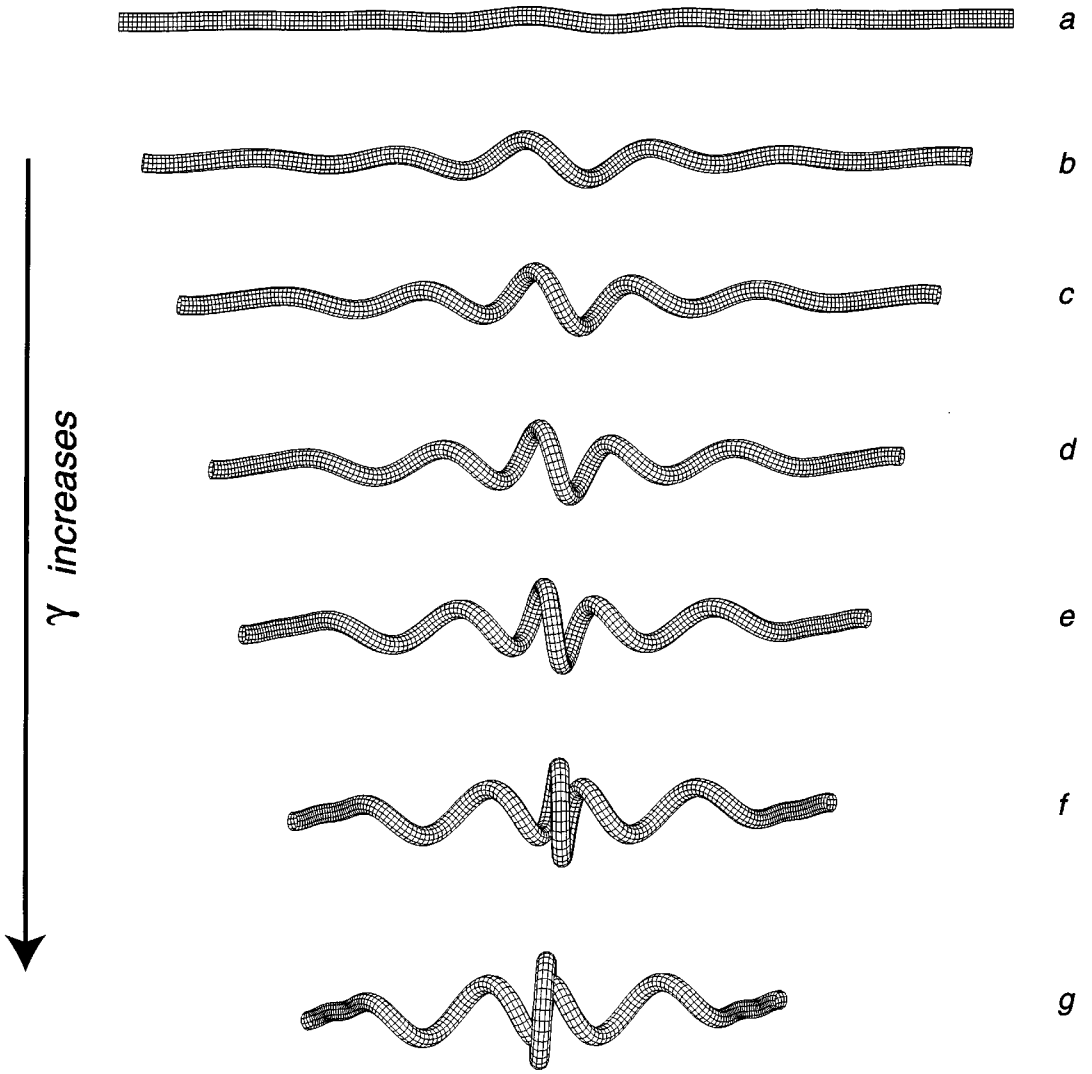

Figure 12. A sequence of helical filaments for varying values of γ_S, (a) $\gamma_S < \gamma_1$, (b) $\gamma_1 < \gamma_S < \gamma_2$, (c) $\gamma_2 < \gamma_S > \gamma_3$, (d) $\gamma_S = \gamma_3$, (e) $\gamma_S > \gamma_3$. The parameters are $\Gamma = 3/4$, $P = 1/10$, $N = 5$, $\gamma_1 = 0.2667$, $\gamma_2 = 0.2684$, $\gamma_3 = 0.27376$, and $\gamma_S = \gamma_2 + \mu$ with $\mu \times 10^3 = 0.1, 1.5, 3, 4.9, 5.36, 5.4$.

7. Morphogenesis Driven by Intrinsic Properties

The most general form of the constitutive relationship (5) includes the presence of intrinsic curvatures, $\kappa_1^{(u)}$ and $\kappa_2^{(u)}$, and intrinsic twist, $\kappa_3^{(u)}$ which determine the 'natural' state of a filament. We now turn to a discussion of the special, if not remarkable, *dynamical* effects that these terms can have in certain biological contexts. The first of these concerns the growth and handedness reversal of tendrils in climbing plants, and the second concerns the self-assembly of certain bacterial filaments.

7.1. Tendril Perversion in Climbing Plants

Tendrils are the tender and flexible side branches of climbing plants, such as the grape-vine, whose circular meanderings (circumnutation) allows the plant to find a support. On contact with, say, a trellis, the tendril's tissues develop in such a way that it starts to curl and tighten up, and acquire a more robust texture. This curling provides the plant with an elastic springlike connection to the support that enables it to withstand high winds and loads. Once the tendril has 'locked' onto the trellis its total twist content cannot change, since neither the main stem or support can rotate. Thus in order to create a (helical) spring out of a filament with essentially zero total twist, the coils of the spiral have to reverse at some point so that the tendril goes from a left-handed helix to a right-handed one, the two being separated by a small segment. This handedness reversal is termed 'perversion' and is Nature's way of creating a 'twistless spring'. The topic of tendril perversion fascinated Charles Darwin who discussed it at length in his charming monograph *The Movements and Habits of Climbing Plants* [44]. In fact, the topic of perversion in plants has a long history and was noted by many eminent botanists. Indeed Linné himself has drawings (Tabula V) of tendrils exhibiting spiral inversion as early as 1751 in his *Philosophia Botannica*.

Tendril perversion is not restricted to plants and is also found to occur in a variety of contexts including the false-twist technique in the textile industry [45]; the microscopic properties of vegetal fibers such as cotton; the formation of bacterial macro-fibers [46]; and in the macrophage scavenger protein, a triple helix with reversed handedness [47]. However, its most familiar – and easily demonstrated – occurrence is in telephone cords: as a coiled telephone cord is first extended and untwisted and then slowly released, a spiral inversion will usually appear in the form of annoying snarls.

A mathematical description of tendril perversion can be provided through a dynamical analysis of the Kirchhoff equations for thin elastic rods in which *intrinsic curvature* plays a special role. The starting point for the analysis is, again, the linear stability of a straight rod: this time the rod is ascribed an intrinsic curvature $\kappa_1^{(u)}$ and a tension P^2. The linear stability analysis yields the dispersion relations

$$\begin{aligned}\Delta \;=\; & -n^6(n^2+P^2)(\Gamma(n^2+P^2)-K^2)-n^4(n^2+P^2)((n^2+1)(2\Gamma-K^2)+2)\sigma^2 \\ & -n^2(n^2+1)((n^2+1)\Gamma+4(n^2+P^2))\sigma^4-2(n^2+1)^2\sigma^6, \end{aligned} \tag{59}$$

where for notational simplicity we have set $\kappa_1^{(u)} \equiv K$. The neutral curves, determined from the condition $\Delta(\sigma = 0, n) = 0$, take the rather simple form

$$(K^2 - \Gamma n^2) = P^2\Gamma. \tag{60}$$

Thus for an infinite rod we see that there exists a critical tension, $P_0 = K/\sqrt{\Gamma}$, such that the rod is unstable for all $P < P_0$. For a finite rod of length L, the first unstable mode is $n = 1/L$ and the corresponding critical tension is $P_1^2 = (L^2K^2 - \Gamma)/(L^2\Gamma)$. We note that $P_1 < P_0$ and that there are a series of decreasing critical tensions associated with the series of (discrete) modes ending with the last possible state which corresponds to the largest integer less than or equal to $KL/\sqrt{\Gamma}$.

To second-order in the perturbation expansion (see Section 3) the solution corresponding to the nth mode takes the form

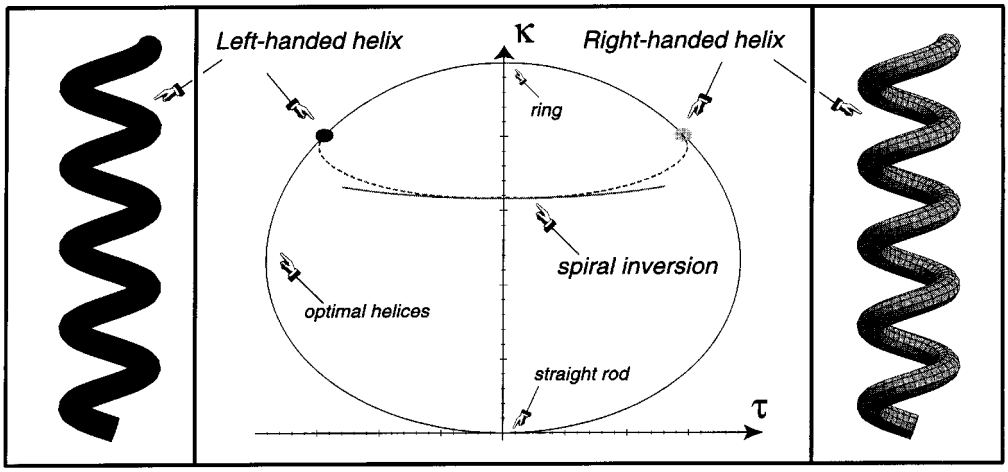

Figure 13. The optimal solution curves in the $\tau_F - \kappa_F$ plane together with the two optimal helices (circles) obtained for $K = 1/4$, $\Gamma = 3/4$,$n = 1/8$ and $P = P_2 \approx 0.286$. The inside curve is the one obtained by the nonlinear analysis for the central piece.

$$x(s,t) = \left(s - X_n^2 \frac{\sin(2ns) + 2ns}{2n}, -2KX_n^2 \frac{P^2\Gamma^2 - K^2(1-\Gamma)\cos^2(ns)}{3P^4\Gamma^2 - 7K^2\Gamma P^2 + 4K^4}, -2X_n \frac{\sin(ns)}{n}\right), \quad (61)$$

where $X_n = \mathrm{Re}(A_n)$. At the level of the linear analysis the amplitude A_n is still, of course, arbitrary and can only be determined by a nonlinear analysis. Carrying this through at the level of a single mode analysis (cf. the discussion of the ring in Section 5) one can determine that the amplitude is

$$A_n^2 = \frac{4\Gamma^{3/2}(P - P_n)(K^2 + 3\Gamma n^2)(K^2 - \Gamma n^2)^{1/2}}{(12 - 7\Gamma)K^4 + 2n^2\Gamma^2(1 - 2\Gamma)K^2 - 3n^4\Gamma^3}. \quad (62)$$

The solution (61) represents the central, perverted, piece of the problem. We argue that this periodic solution is close to the heteroclinic solution that asymptotically connects helices of opposite handedness, and using the above results and the standard properties of helices (see Section 4) we can show that these helices have a Frenet torsion $\tau_F^2 = (P^2\kappa_F)/(K + \kappa_F(\Gamma - 1))$, and a Frenet curvature, κ_F, satisfying the condition

$$2(\Gamma - 1)\kappa_F^3 - 2K(\Gamma - 2)\kappa_F^2 - 2\kappa_F K^2 + \Gamma\tau_F^2 K = 0.$$

From these calculations a rather nice picture tendril perversion emerges. As the tension decreases for a given intrinsic curvature (or equivalently for an increasing intrinsic curvature and given tension), the tendril reaches a critical state where it looses stability and bifurcates into a solution exhibiting perversion. Beyond threshold this solution asymptotically connects to helical solutions of opposite handedness and specific geometry. As shown in Figure 13 this family of helices forms a closed curve passing through the points $(0, 0)$ (straight line) and $(K, 0)$ (rings). Each point on the curve represents a helix for given P, K, Γ. The perverted filament asymptotically connects two optimal helices: a right-handed one ($\tau_F > 0$) to a left-handed one ($\tau_F < 0$)). This figure suggests that the perverted filament is, in fact, a heteroclinic orbit in the curvature-torsion plane joining two asymptotic fixed points (corresponding to the two helices).

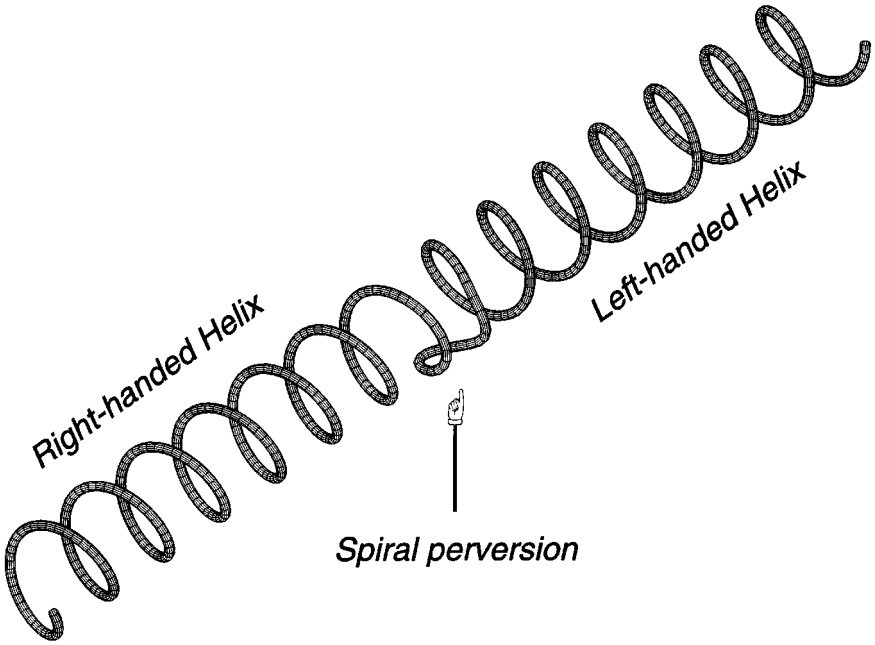

Figure 14. Sketch of a helix hand reversal.

7.2. SELF-ASSEMBLY OF *Bacillus subtilis*

The individual cells of the bacterial strain *Bacillus subtilis* are rod-shaped and typically of length 3–4 μm and diameter 0.8 μm. Under certain circumstances they are found to grow into filaments consisting of the cells linked in tandem due to the failure of daughter cells, produced by growth and septation, to separate [5]. As they elongate these filaments, which are immersed in a liquid environment (whose temperature and viscosity can be controlled), are observed to twist at uniform rate. The degree of twist and handedness can, in fact, be controlled experimentally and a wide range of states from left-handed to right-handed forms, can be produced. The actual twist state of the cells seems to be related to properties of the polymers which are inserted into the cell wall during growth. As they elongate the filaments are observed to whirl and writhe and eventually deform into double-helical structures. These continue to grow and periodic repetition of this process results in macroscopic fibers (termed 'macro-fibers') with a specific twist state and handedness. (A schematic representation of this dynamics is given in Figure 15.) A striking feature of this iterated process is that at every stage of the self-assembly, the handedness of the helical structures that are created is the *same* (e.g. a right-handed double helix gives rise to a right-handed four-strand helix and so on). The nature of the environment does, however, influence certain aspects of the self-assembly. In a viscous environment the basic writhing instability leads to something of a 'buckling' at the middle of the filament with the formation of a tight central loop; this is followed by a helical wind-up which starts at the base of this loop. By contrast, in a non-viscous medium, the instability causes the filament to fold over into a large loop closed by contact between the ends of the filament. This closure is then followed by a helical wind-up starting at that point. In both cases this self-assembly conserves handedness and usually continues over long periods until macro-fibers, several millimeters long, are formed.

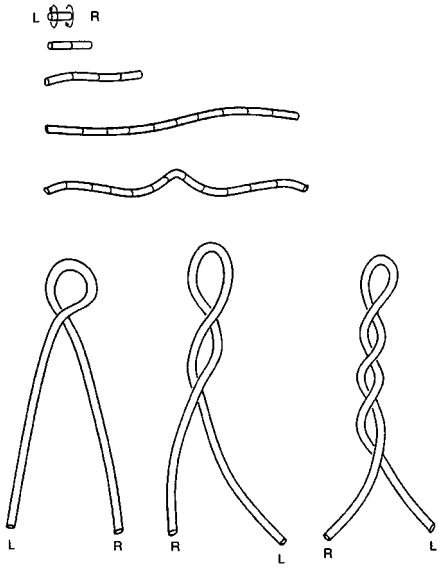

Figure 15. An elementary twist to writhe conversion in growing *Bacillus subtilis*.

Due its structural complexity, the fact that it grows, and the presence of a fluid environment, mathematical modeling of *Bacillus subtilis* dynamics presents many challenges (see, for instance, [48]). Nonetheless, some progress can be made using many of the ideas described above. One fundamental clue to developing a model lies in the observed, handedness preserving, twist-to-writhe conversion. Since the dynamics of this conversion is so fundamental we begin our discussion by first considering the following elementary demonstration involving the twisting of an elastic rubber tube with circular cross-section. Held out straight the tube can be said to be a 'naturally' straight rod, i.e. its relaxed lowest energy state is that of a straight rod without any twist or curvature. The tube is held in both hands and twisted, say, with right-handed twist. The straight line markers can be seen to take on a left-handed helical path showing that the total twist of the rod is now greater than zero. To return to its natural state the excess twist must be removed. One way to do this is simply to let go of one end, which allows the tube to relax by unwinding in the counter-clockwise sense. This unwinding takes the form of a *twist wave* propagating along the tube from the free end towards the fixed end. It should be noted that these twist waves correspond to fairly large-scale 'whirling' or 'crankshaft' like motions in which the tube undergoes quite substantial lateral deformations as it turns. Relief of twist can also be achieved without allowing either end to rotate freely; namely by letting the restrained ends approach each other and a supercoil form in the counter-clockwise (left-handed) sense. This is the most elementary form of twist-to-writhe conversion. Despite its convoluted structure the total twist of the tube when supercoiled is returned almost to zero which corresponds to the equilibrium energy state. However, for a fundamental reason, this example differs from the situation in *Bacillus subtilis*, and DNA, where an initial form of a given handedness gives rise to a supercoiled structure that is of the *same* handedness. This fundamental difference in behavior is due to the presence of an 'intrinsic' twist in the filament. To illustrate this consider a rubber tube with left-handed intrinsic twist (see Figures 16 and 17). The straightened tube is then twisted at one end in the opposite direction until the markers are approximately straightened out. The current twist density of the filament in this state

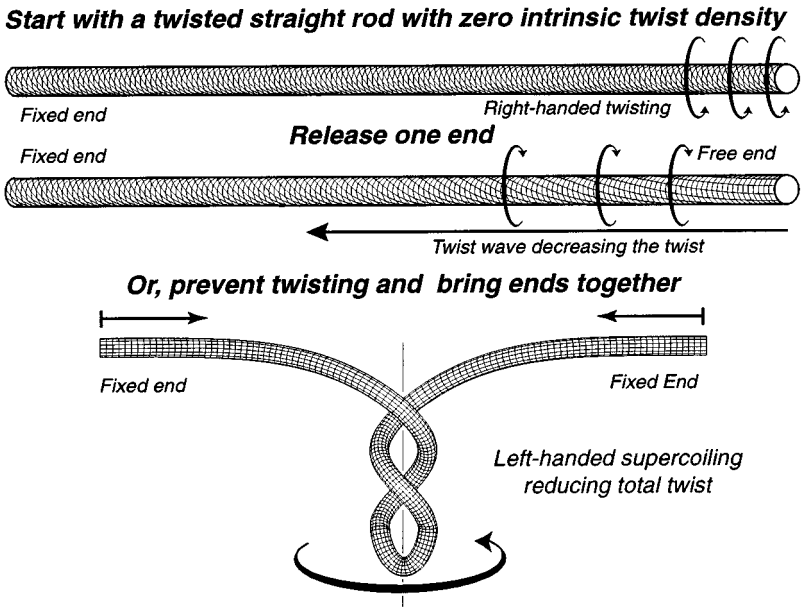

Figure 16. Twist to writhe conversion with no intrinsic twist.

would appear to be zero but its natural state is one of non-zero twist density as indicated by the original helical marker lines. To achieve its natural state the tube must make up for the (apparent) 'twist deficit'. If one end is freed the tube winds in a clockwise sense (the same as the helical marker lines) again sending a twist wave down the rod. If the ends are not freed but brought towards each other, the tube will supercoil to relax. In this case the supercoiling is with the *same* handedness as the intrinsic twist.

For the purpose of modeling the bacterial strands we assume that each individual bacterial cell is a segment of an elastic filament and that it possess an 'intrinsic' twist κ_3^u. Growth of all the cells in a filament uniformly results in an exponential growth accompanied by a gradual reduction of the local twist density. Returning to the rubber tube model described earlier, the intrinsic twist is represented by a helical marker line on the surface of the filament. As the filament grows exponentially the marker line constantly changes pitch as if straightening out along the filament length. Changing pitch in this direction away from the initial twist, κ_3^u, results in a filament that can be considered undertwisted. The greatest twist deficit, measured by $\kappa_3 - \kappa_3^u$ (i.e. the difference between the local twist density and the intrinsic twist), will be found in the central portion of the filament whereas the twist deficit will be smallest at the filament ends. This results in a large twist gradient at the center of the filament which therefore produces an axial torque. This creates a whirling instability at each of the free ends – in principle these whirling motions propagate twist back to the center of the filament until the twist deficit has been eliminated. However, two competing processes come into play:

1. the continuous growth of the filament provides an ongoing source of torque at the filament center;
2. due to the growth, the whirling portions of the filament increase in length and experience an ever increasing drag exerted by the fluid medium.

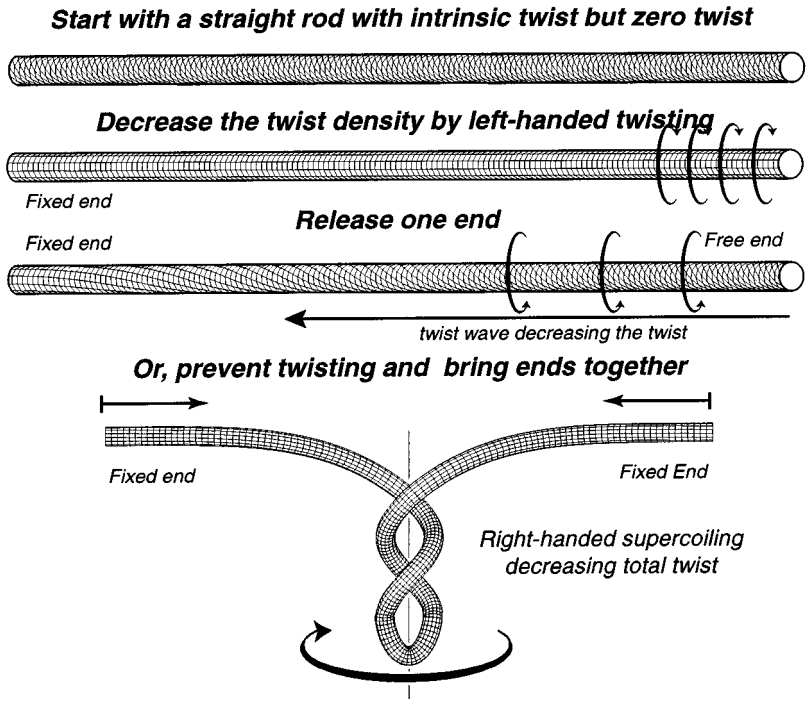

Figure 17. Twist to writhe conversion with intrinsic twist.

At a certain point the central, growth produced, torque (one can think of the central portion of the filament as a 'torque engine' fueled by the growth) cannot overcome the viscous drag. The whirling motions are effectively blocked and the sort instability scenarios for twisted straight rods that we have discussed take over. Now, as the rod continues to grow, the twist deficit builds up and, without the possibility of relief from whirling motions at the ends, undergoes a supercoiling, *with the same handedness*, to eliminate the twist deficit.

A more quantitative picture has proved to be rather difficult to develop. However, some simple scaling arguments can be proposed. For example, based on crude estimates of balance between the torque generated by filament growth and the drag experienced by the whirling portions, suggests that the critical buckling length might behave as

$$l_* \sim \left(\frac{\mu J \kappa_3^u}{C\eta r}\right)^{1/3}, \tag{63}$$

where η is the dynamic viscosity of the fluid medium, r the filament growth rate, μ the shear modulus and J the axial moment of the filament, and C an unknown coefficient related to the drag. The scaling $l_* \sim \eta^{-1/3}$ is not intuitively obvious.

Acknowledgments

This work is supported by the Flinn Foundation, NSF grant DMS-9704421, NSF grant DMS-9972063 and NATO-CRG 97/037. Alain Goriely is a Sloan Fellow. The authors would like to thank Neil Mendelson for letting them use Figure 15.

References

1. Zajac, E. E., 'Stability of two planar loop elasticas', *Transactions of the ASME*, March, 1962, 136–142.
2. Coyne, J., 'Analysis of the formation and elimination of loops in twisted cable', *IEE Journal of Oceanic Engineering* **15**, 1990, 72–83.
3. Barkley, M. D. and Zimm, B. H., 'Theory of twisting and bending of chain macromolecules; Analysis of the fluorescence depolorization of DNA', *Journal of Chemical Physics* **70**, 1979, 2991–3006.
4. Benham, C. J., 'Theoretical analysis of conformational equilibria in superhelical DNA', *Annual Review of Biophysical Chemistry* **14**, 1985, 23–45.
5. Mendelson, N. H., 'Bacterial macrofibers: The morphogenesis of complex multicellular bacterial forms', *Scientific Progress Oxford* **74**, 1990, 425–441.
6. Thwaites, J. J. and Mendelson, N. H., 'Mechanical behavior of bacterial cell walls', *Advances in Microbiological Physiology* **32**, 1991, 174–222.
7. Hunt, N. G. and Hearst, J. E., 'Elastic model of DNA supercoiling in the infinite length limit', *Journal of Chemical Physics* **12**, 1991, 9329–9336.
8. Schlick, T. and Olson, W. K., 'Trefoil knotting revealed by molecular dynamics simulations of supercoiled DNA', *Science* **257**, 1992, 1110–1114.
9. Yang, Y., Tobias, I., and Olson, W. K., 'Finite element analysis of DNA supercoiling', *Journal of Chemical Physics* **98**, 1993, 1673–1686.
10. Bauer, W. R., Lund, R. A., and White, J. H., 'Twist and writhe of a DNA loop containing intrinsic bends', *Proceedings of the National Academy of Science (USA)* **90**, 1993, 833–837.
11. Shi, Y. and Hearst, J. E., 'The Kirchhoff elastic rod, the nonlinear Schrödinger equation and DNA supercoiling', *Journal of Chemical Physics* **101**, 1994, 5186–5200.
12. Goldstein, R. E. and Langer, S. A., 'Nonlinear dynamics of stiff polymers', *Physical Review Letters* **75**, 1995, 1094.
13. Shelley, M. J. and Ueda, T., 'The nonlocal dynamics of stretching, buckling filaments', in *Advances in Multi-Fluid Flows*, D. Papageorgiou and Y. Renardi (eds.), SIAM, Philadelphia, PA, 1996, pp. 415–425.
14. Keener, J. P., 'Knotted vortex filament in an ideal fluid', *Journal of Fluid Mechanics* **211**, 1990, 629–651.
15. Spruit, H. C., 'Motion of magnetic flux tubes in the solar convection zone and chromosphere', *Astronomy and Astrophysics* **98**, 1981, 155.
16. Da Silva, S. and Chouduri, A. R., 'A theoretical model for tilts of bipolar magnetic regions', *Astronomy and Astrophysics* **272**, 1993, 621.
17. Thompson, J. M. T. and Champneys, A. R., 'From helix to localized writhing in the torsional post-buckling of elastic rods', *Proceedings of Royal Society of London Series A* **452**, 1996, 117–138.
18. Schlick, T., 'Modeling superhelical DNA: Recent analytical and dynamical approaches', *Current Opinions in Structural Biology* **5**, 1995, 245–262.
19. Dill, E. H., 'Kirchhoff's theory of rods', *Archives of the History of Exact Science* **44**, 1992, 2–23.
20. Love, A. E. H., *A Treatise on the Mathematical Theory of Elasticity*, Cambridge University Press, Cambridge, 1892.
21. Landau, L. D. and Lifshitz, E. M., *Theory of Elasticity*, Pergamon Press, Oxford, 1959.
22. Timoshenko, S. P. and Gere, J. M., *Theory of Elastic Stability*, McGraw-Hill, New York, 1961.
23. Coleman, B. D. and Dill, E. H., 'Flexure waves in elastic rods', *Journal of Acoustical Society of America* **91**, 1992, 2663.
24. Tanaka, F. and Takahashi, H., 'Elastic theory of supercoiled DNA', *Journal of Chemical Physics* **11**, 1985, 6017–6026.
25. Tsuru, H., 'Equilibrium shapes and vibrations of thin elastic rod', *Journal of the Physical Society of Japan* **56**, 1987, 2309–2324.
26. Maddocks, J. H. and Dichmann, D. J., 'Conservation laws in the dynamics of rods', *Journal of Elasticity* **34**, 1994, 83–96.
27. Klapper, I. and Tabor, M., 'Dynamics of twist and writhe and the modeling of bacterial fibers', *Mathematical Approaches to Biomolecular Structure and Dynamics*, J. Mesirov, K. Schuiten, and D. W. Summers (eds.), Springer-Verlag, New York, 1996, pp. 139–159.
28. Klapper, I., 'Biological applications of the dynamics of twisted elastic rods', *Journal of Computational Physics* **125**, 1996, 325–337.

29. Goriely, A. and Tabor, M., 'New amplitude equations for thin elastic rods', *Physical Review Letters* **77**, 1996, 3537–3540.
30. Goriely, A. and Tabor, M., 'Nonlinear dynamics of filaments I: Dynamical instabilities', *Physica D* **105**, 1997, 20–44.
31. Goriely, A. and Tabor, M., 'Nonlinear dynamics of filaments II: Nonlinear analysis', *Physica D* **105**, 1997, 45–61.
32. Goriely, A. and Tabor, M., 'Nonlinear dynamics of filaments III: Instabilities of helical rods', *Proceedings of the Royal Society of London Series A* **453**, 1997, 2583–2601.
33. Goriely, A. and Tabor, M., 'Nonlinear dynamics of filaments IV: Spontaneous looping', *Proceedings of the Royal Society of London Series A* **455**, 1998, 3183–3202.
34. Goriely, A., Nizette, M., and Tabor, M., 'On the dynamics of elastic strips', *Journal of Nonlinear Science*, 1999, submitted.
35. Coleman, B. D., Dill, E. H., Lembo, M., Lu, Z., and Tobias, I., 'On the dynamics of rods in the theory of Kirchhoff and Clebsch', *Archives for Rational Mechanics and Analysis* **121**, 1993, 339–359.
36. Goriely, A., Mendelson, N., and Tabor, M., 'Dynamical buckling of *Bacillus subtilis*', Preprint, 1998.
37. Goriely, A. and Tabor, M., 'Spontaneous helix-hand reversal and tendril perversion in climbing plants', *Physical Review Letters* **80**, 1998, 1564–1567.
38. Newell, A., *Envelope Equations*, Lectures in Applied Mathematics, Vol. 15, American Mathematical Society, Providence, RI, 1974.
39. Rogers, K. A., 'Stability exchange in parameter dependent constrained variational principles with applications to elastic rod models os DNA minicircles', University of Maryland, Ph.D. Thesis, 1997.
40. Kehrbaum, S. and Maddocks, J. H., 'Effective properties of elastic rods with high intrinsic twist', Preprint, 1997.
41. Goriely, A. and Lega, J., 'Pulses, fronts and oscillations of an elastic rod', *Physica D*, 1998, to be published.
42. Weiss, J., Tabor, M. and Carnevale, G., 'The Painlevé property for partial differential equations', *Journal of Mathematical Physics* **24**, 1983, 3.
43. Champneys, A. R., van der Heiden, G. H. M., and Thompson, J. M. T., 'Spatially complex localisation after one-twist-per-wave equilibria in twisted rod circular rods with initial curvature', *Philosophical Transactions of the Royal Society of London Series A* **355**, 1988, 2151–2174.
44. Darwin, Ch., *The Movements and Habits of Climbing Plants*, Appleton, New York, 1888.
45. Hearle, J. W. S., Thwaites, J. J., and Amirbayat, J. (eds.), *Mechanics of Flexible Fibre Assemblies*, Sijthoff & Noordhoff, Germantown, 1980.
46. Tilby, M. J., 'Helical shape and wall synthesis in bacterium', *Nature* **266**, 1977, 450–452.
47. Galloway, J. W., 'Macromolecular asymmetry', in *Biological Asymmetry and Handedness*, G. R. Bock and J. Marsh (eds.), Wiley-Interscience, New York, 1991, pp. 16–35.
48. Goldstein, R. E., Powers, T. R., and Wiggins, C. H., 'Viscous nonlinear dynamics of twist and writhe', *Physical Review Letters* **80**, 1998, 5232–5235.